Nascent RNA antagonizes the interaction of a set of regulatory proteins with chromatin

Graphical abstract
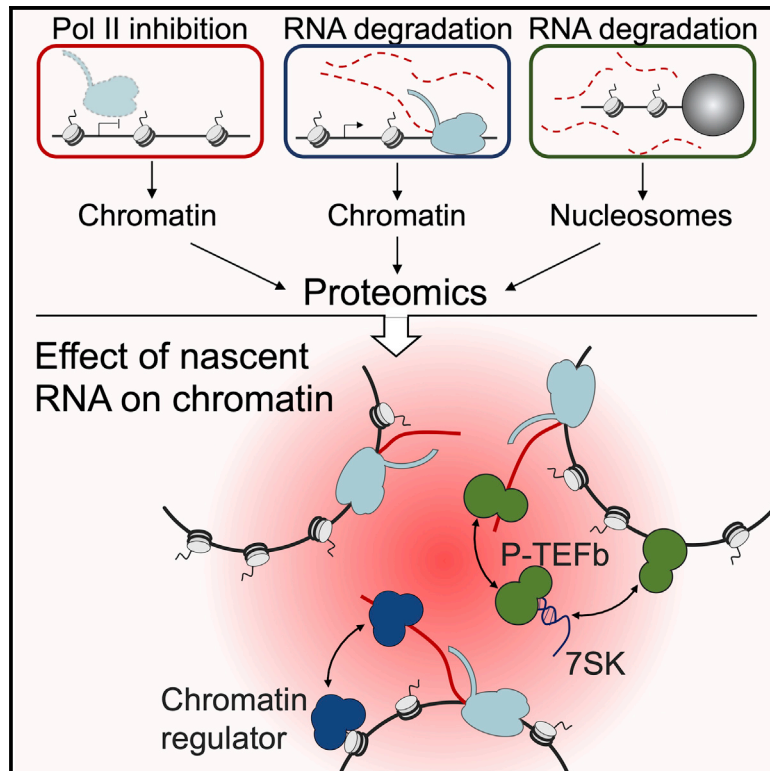
Authors

Lenka Skalska, Victoria Begley,
Manuel Beltran, ...,
Ambrosius P. Snijders, Till Bartke,
Richard G. Jenner

Correspondence

r.jenner@ucl.ac.uk

In brief

Nascent RNA interacts with a wide array of regulatory proteins but its impact on chromatin composition has not been assessed. Skalska and colleagues use proteomics methods to reveal that nascent RNA antagonizes the association of a set of regulatory proteins with chromatin.

Highlights

- Pol II inhibition induced recruitment of a set of regulatory proteins to chromatin

- Many of these changes were also observed upon RNA degradation

- RNA binds a set of chromatin modifiers and inhibits interaction with nucleosomes

- P-TEFb binds pre-mRNA, and 7SK regulates its interaction with RNA and chromatin

Article

Nascent RNA antagonizes the interaction of a set of regulatory proteins with chromatin

Lenka Skalska,[1,6,7] Victoria Begley,[1,6] Manuel Beltran,[1,6,8] Saulius Lukauskas,[2] Garima Khandelwal,[1] Peter Faull,[3,9] Amandeep Bhamra,[5] Manuel Tavares,[1] Rachel Wellman,[1] Andrey Tvardovskiy,[2] Benjamin M. Foster,[2,10] Igor Ruiz de los Mozos,[3,4] Javier Herrero,[1] Silvia Surinova,[5] Ambrosius P. Snijders,[3] Till Bartke,[2] and Richard G. Jenner[1,11,*]

[1]UCL Cancer Institute and Cancer Research UK UCL Centre, University College London (UCL), London WC1E 6BT, UK
[2]Institute of Functional Epigenetics, Helmholtz Zentrum München, Neuherberg 85764, Germany
[3]The Francis Crick Institute, London NW1 1AT, UK
[4]Institute of Neurology, UCL, London WC1N 3BG, UK
[5]Proteomics Research Translational Technology Platform, UCL Cancer Institute and Cancer Research UK UCL Centre, University College London (UCL), London WC1E 6BT, UK
[6]These authors contributed equally
[7]Present address: Barking, Havering, and Redbridge University Hospitals NHS Trust, Romford, UK
[8]Present address: Department of Biology and Biotechnology Charles Darwin, Sapienza University of Rome, Rome, Italy
[9]Present address: College of Pharmacy, The University of Texas at Austin, Austin, TX 78712, USA
[10]Present address: Department of Biochemistry, University of Oxford, Oxford, UK
[11]Lead contact
*Correspondence: r.jenner@ucl.ac.uk
https://doi.org/10.1016/j.molcel.2021.05.026

SUMMARY

A number of regulatory factors are recruited to chromatin by specialized RNAs. Whether RNA has a more general role in regulating the interaction of proteins with chromatin has not been determined. We used proteomics methods to measure the global impact of nascent RNA on chromatin in embryonic stem cells. Surprisingly, we found that nascent RNA primarily antagonized the interaction of chromatin modifiers and transcriptional regulators with chromatin. Transcriptional inhibition and RNA degradation induced recruitment of a set of transcriptional regulators, chromatin modifiers, nucleosome remodelers, and regulators of higher-order structure. RNA directly bound to factors, including BAF, NuRD, EHMT1, and INO80 and inhibited their interaction with nucleosomes. The transcriptional elongation factor P-TEFb directly bound pre-mRNA, and its recruitment to chromatin upon Pol II inhibition was regulated by the 7SK ribonucleoprotein complex. We postulate that by antagonizing the interaction of regulatory proteins with chromatin, nascent RNA links transcriptional output with chromatin composition.

INTRODUCTION

It is well established that the transcription of DNA into coding and non-coding RNAs (ncRNAs) is regulated by proteins that respond to DNA sequence composition and chromatin state. It is also becoming clear that RNA molecules can themselves play a role in transcriptional and chromatin regulation. This was first demonstrated in mammalian cells for the transactivation response element (TAR), an RNA stem-loop formed at the 5′ end of nascent HIV transcripts, and for the cellular ncRNA, 7SK. TAR binds the HIV transactivator protein Tat, and these factors act together to release the positive transcription elongation factor b (P-TEFb) from the inhibitory 7SK ribonucleoprotein (RNP) complex to activate HIV transcriptional elongation (Barboric et al., 2007; Garber et al., 1998; Michels et al., 2003; Sedore et al., 2007; Wei et al., 1998; Yik et al., 2003). Since then, a number of long non-coding RNAs (lncRNAs) and enhancer RNAs (eRNAs) have been found to interact with transcriptional and chromatin regulatory proteins and modulate their recruitment or activity at specific sites on chromatin (Rinn and Chang, 2012).

In addition to the functions of specialized ncRNAs, RNA also acts in a global manner to regulate chromatin state. RNA and transcription affect higher-order structure across the genome (Barutcu et al., 2019; Heinz et al., 2018; Li et al., 2015; Saldaña-Meyer et al., 2019). Building on models in which RNA forms a static nuclear matrix (Nickerson et al., 1989), it was more recently proposed that pre-mRNAs and other nascent transcripts form a dynamic nuclear RNA matrix that holds open active chromatin (Nozawa et al., 2017). Consistent with a more general role for RNA in chromatin regulation, recent studies demonstrate that chromatin regulators interact with a wide array of nascent transcripts. Although first identified to bind specific ncRNAs, polycomb repressive complex 2 (PRC2), DNMT1 and DNMT3A, LSD1/KDM1A, CBX3, YY1, HDAC1, and CHD4 primarily interact with nascent pre-mRNAs
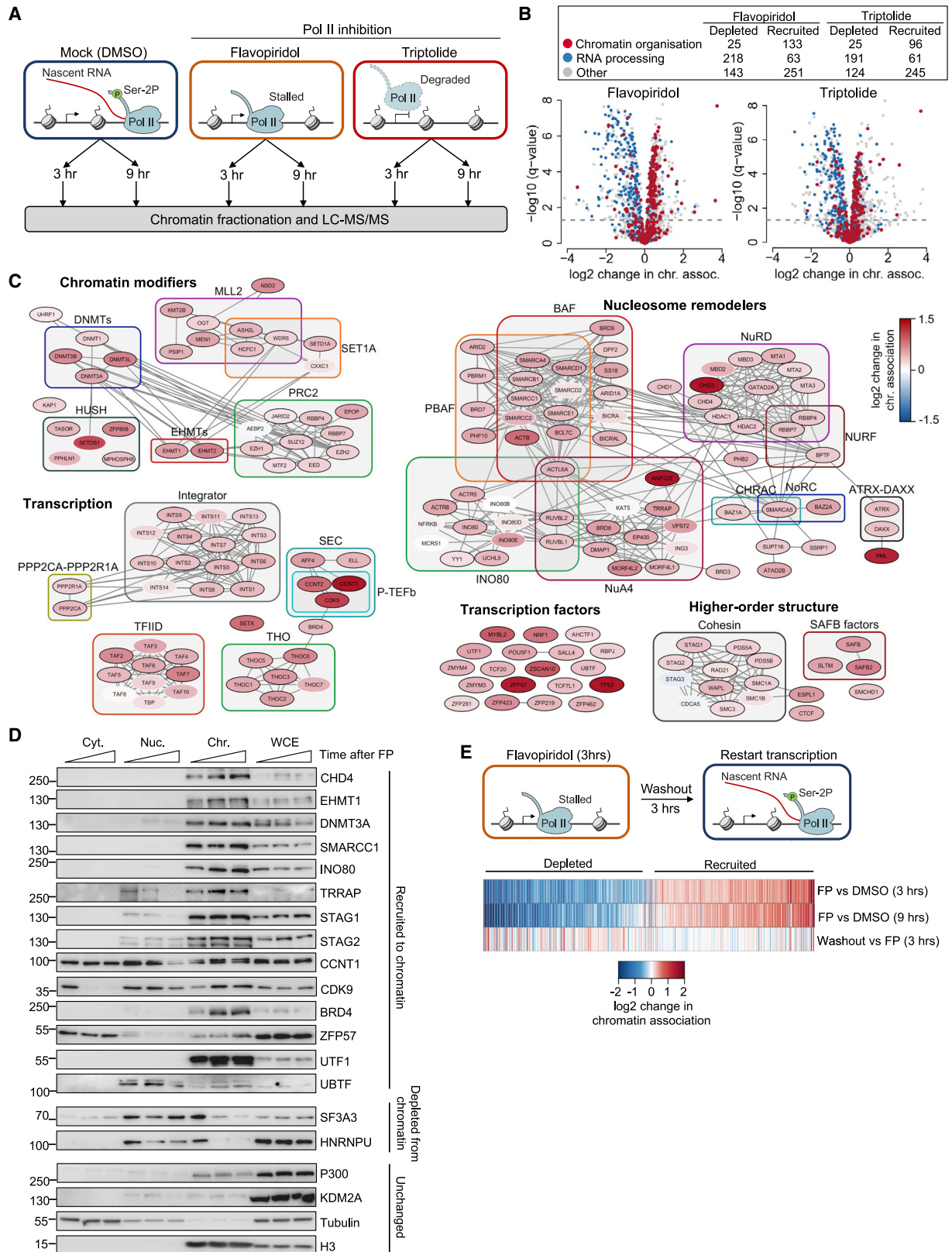
(Beltran et al., 2016; Hendrickson et al., 2016; Kaneko et al., 2013; Savell et al., 2016; Sigova et al., 2015). Similarly, unbiased screens for proteins interacting with nascent RNA or non-polyadenylated transcripts in cells have revealed enrichment for chromatin regulators (Bao et al., 2018; He et al., 2016; Trendel et al., 2019).

For the majority of factors identified to bind RNA in cells, the effect on their association with chromatin has not been determined. Although RNAs have primarily been considered to recruit regulatory proteins to chromatin, it has become apparent that nascent RNA can antagonize the association of proteins with chromatin. This is best understood for the repressive chromatin modifier PRC2. PRC2 directly interacts with pre-mRNAs at essentially all active genes (Beltran et al., 2016; Davidovich et al., 2013; Kaneko et al., 2013) but preferentially binds G-quadruplex (G4)-forming sequences within these transcripts (Beltran et al., 2019; Kaneko et al., 2014; Wang et al., 2017a). *In vitro*, RNA competes with nucleosomes for PRC2 binding and inhibits PRC2 catalytic activity (Beltran et al., 2016, 2019; Cifuentes-Rojas et al., 2014; Herzog et al., 2014; Kaneko et al., 2014; Wang et al., 2017b; Zhang et al., 2019). In cells, blocking RNA polymerase II (RNA Pol II) transcription (Hosogane et al., 2016; Kaneko et al., 2014; Riising et al., 2014) or degrading RNA (Beltran et al., 2016) triggers PRC2 recruitment to active genes. Reciprocally, blocking nuclear RNA degradation (Garland et al., 2019) or tethering G4-forming RNAs to repressed genes (Beltran et al., 2019) removes PRC2 from chromatin. Thus, pre-mRNA regulates its own production by preventing the recruitment of PRC2 to chromatin at active genes (Skalska et al., 2017). However, the broader impact of nascent RNA on the interaction of proteins with chromatin has not been determined.

We used proteomics methods to determine the effect of nascent RNA on the interaction of proteins with chromatin in embryonic stem cells (ESCs). Unexpectedly, we found that nascent RNA primarily acted to inhibit the interaction of chromatin and transcriptional regulatory proteins with chromatin. We further demonstrate that nascent pre-mRNA directly binds to P-TEFb and that the 7SK RNP regulates the interaction of P-TEFb with nascent RNA and chromatin.

RESULTS

A set of regulatory proteins are recruited to chromatin upon transcriptional inhibition

We sought to determine the impact of RNA Pol II transcription of nascent RNA on the association of proteins with chromatin using a stable isotope labeling with amino acids in cell culture (SILAC)-based quantitative proteomics approach. Mouse ESCs were treated with the transcription factor II human (TFIIH) inhibitor triptolide, which blocks transcriptional initiation and leads to RNA Pol II degradation, or the CDK9 inhibitor flavopiridol, which blocks transcriptional elongation, for 3 or 9 h (Figures 1A and S1A). These time points were chosen due to the previous observation that PRC2 was recruited to chromatin in ESC after 9 h of treatment with triptolide (Riising et al., 2014). RNA sequencing (RNA-seq) revealed that flavopiridol and triptolide treatments had a greater effect on chromatin-associated nascent RNA (rRNA-depleted intronic reads) than on mature polyA+ exonic RNA and that transcription had largely ceased by 9 h (Figures S1B and S1C). Chromatin fractions were purified and verified by silver stain and immunoblotting (Figures S1D and S1E). The constituent proteins were then quantified by liquid chromatography-tandem mass spectrometry (LC-MS/MS) relative to chromatin from DMSO-treated cells at the same time point.

This analysis revealed a set of proteins lost from chromatin upon RNA Pol II inhibition and, unexpectedly, a set of proteins recruited to chromatin upon RNA Pol II inhibition (Figure 1B; Table S1). These changes were observed upon treatment with both flavopiridol and triptolide ($r = 0.66$, $p = 2.9 \times 10^{-196}$, Pearson correlation and t test), and similar changes were evident at 3 and 9 h for both flavopiridol ($r = 0.53$, $p = 8 \times 10^{-108}$) and triptolide ($r = 0.62$, $p = 4.3 \times 10^{-162}$) (Figure S1F). The changes were not due to the indirect effects of transcriptional inhibition on the cell cycle; treatment with flavopiridol and triptolide had similar effects on chromatin but opposite effects on the relative proportions of cells in G1 versus M phase (Figure S1G). Similarly, RNA Pol II inhibition had little effect on apoptosis (Figure S1H) or DNA damage signaling (γH2A.X; Figure S1I), especially at the 3-h time point. Similar effects could be observed after a 1-h treatment with flavopiridol and with a lower drug concentration (Figure S1J), again,

---

Figure 1. A set of regulatory proteins are recruited to chromatin upon transcriptional inhibition

(A) Experimental strategy. ESCs were treated with DMSO, flavopiridol, or triptolide for 3 or 9 h, the chromatin fractions purified, and proteins quantified relative to DMSO by SILAC.

(B) Significance (q value/FDR) of changes in the association of proteins with chromatin upon treatment with flavopiridol (left) or triptolide (right) versus DMSO at 9 h. The GO term RNA processing (blue) was significantly enriched ($p = 8.9 \times 10^{-52}$, hypergeometric) in the set of proteins depleted from chromatin (FDR < 0.05) in both treatments. The GO term Chromatin Organization (red) was significantly enriched ($p = 4 \times 10^{-5}$) in the set of proteins recruited to chromatin (FDR < 0.05). Proteins with these functions are highlighted and their frequencies within the sets of proteins recruited or depleted from chromatin shown above.

(C) Proteins that exhibited significantly increased abundance in the chromatin fraction upon RNA Pol II inhibition with flavopiridol and triptolide (9 h). Protein complexes are labeled if a significant proportion of their subunits were increased on chromatin (p < 0.05, hypergeometric). Interactions between proteins (STRING) are shown as lines. Changes in the chromatin association of individual proteins upon treatment with flavopiridol are indicated by color, according to the scale on the right, and by the outline (black FDR < 0.05, white FDR > 0.05).

(D) Immunoblots for proteins representative of those shown in (C) in the cytoplasmic, nucleoplasmic, and chromatin fractions and whole-cell extract (WCE) taken from ESCs after 0, 3, or 6 h of incubation with flavopiridol.

(E) Top, strategy: after the 3-h incubation, flavopiridol was washed out, cells incubated for a further 3 h, and then harvested. Bottom: proteins either recruited to or depleted from chromatin (FDR < 0.05) upon treatment with flavopiridol at the 3-h time point (n = 519) ordered by the change in chromatin binding (average of 3- and 9-h time points). Changes in chromatin association induced by flavopiridol washout (relative to 3-h flavopiridol) are shown below and are anti-correlated with the changes initially induced by flavopiridol ($r = -0.34$, 8.5×10^{-16}, n = 519). Changes in chromatin association are colored according to the scale beneath. See also Figure S1 and Tables S1 and S2.
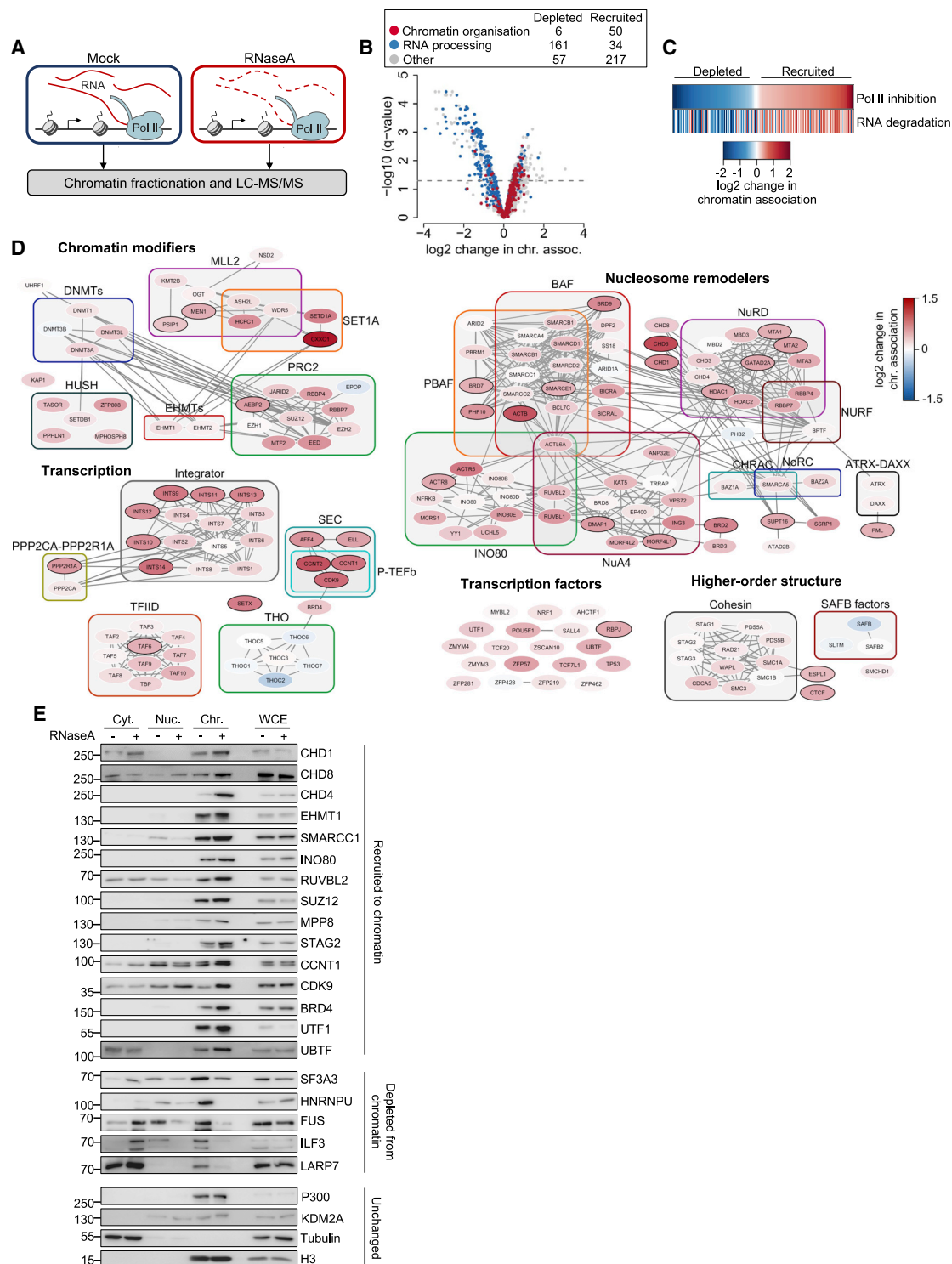
Figure 2. RNA degradation has similar effects to RNA Pol II inhibition on the interaction of proteins with chromatin

(A) Experimental strategy. ESCs were permeabilized, mock-treated or treated with RNaseA to degrade RNA, chromatin fractions purified, and proteins quantified by label-free LC-MS/MS.

(B) Significance of changes in the association of proteins with chromatin upon RNaseA treatment versus mock-treated control. Proteins with functions in RNA processing and chromatin organization are highlighted in blue or red, respectively, and their frequencies in the sets of proteins recruited or depleted from chromatin (FDR < 0.05) shown above.

(legend continued on next page)

consistent with changes being a direct effect of transcriptional inhibition.

We examined the set of proteins significantly depleted (false discovery rate [FDR] < 0.05) from chromatin upon RNA Pol II inhibition with both flavopiridol and with triptolide (9 h; n = 241). As may be expected, this revealed enrichment of proteins with functions in RNA processing (Gene Ontology [GO]: 0006396; p = 8.9×10^{-52}, hypergeometric), including significant enrichment of subunits of the spliceosome, exosome, polyA complex, exon junction complex, and RNA Pol II-bound factors such as the PAF complex and SPT6/ISW1 (Figures 1B and S1K; Table S2). These proteins also included HNRNPU, previously shown to interact with chromatin in an RNA-dependent manner (Nozawa et al., 2017). Thus, these factors act as positive controls and suggest that the observed changes are caused by the loss of RNA Pol II transcription.

We then turned our attention to the set of proteins recruited to chromatin upon RNA Pol II inhibition with both flavopiridol and triptolide (n = 281). We found an enrichment of factors with roles in chromatin organization (GO: 0006325; p = 4×10^{-5}), gene expression (Reactome [REAC]: R-MMU-74160; p = 6×10^{-4}), and ESC pluripotency (WP: PluriNetWork; p = 5×10^{-12}) (Figures 1B and S1K; Table S2). A number of complexes exhibited a significant enrichment of subunits (p < 0.05, hypergeometric) in the set of proteins recruited to chromatin upon RNA Pol II inhibition (Figure 1C; Table S2). These included PRC2, which has previously been shown to be recruited to chromatin upon transcriptional inhibition (Riising et al., 2014), other chromatin modifiers (DNMTs, EHMT1/2, MLL2/SET1A, HUSH), nucleosome remodelers (NuRD, NURF, NoRC, CHRAC, NuA4, INO80, BAF, ATRX/DAXX), regulators of higher-order structure (cohesin, CTCF, SMCHD1, SAFB), and transcription factors (including POU5F1 [OCT4], ZFP57, UBTF, TP53, MYBL2 and UTF1). Surprisingly, we also found that a number of regulators of RNA Pol II processivity, including P-TEFb and other components of the super-elongation complex (SEC), PPP2C1 (PP2A), BRD4, and Integrator, were recruited to chromatin upon RNA Pol II inhibition, with P-TEFb exhibiting particularly large increases in chromatin association (Figure 1C). Immunoblotting for representative proteins in cell fractions generated using a different biochemical method confirmed RNA Pol II inhibition induced changes in chromatin association for 16 of the 22 proteins tested (73%) and validated that changes in chromatin association were not an artifact of changes in total protein abundance (Figure 1D; Table S1).

We considered that if the changes in the association of proteins with chromatin were the direct effects of changes in transcription, then restarting transcription should begin to reverse the changes. We therefore also analyzed cells harvested 3 h after flavopiridol had been washed out after the initial 3-h incubation (Figures 1E and S1L). This showed that removing flavopiridol

and allowing transcriptional elongation to restart began to reverse the changes caused by flavopiridol treatment (r = −0.34, p = 8.5×10^{-16}), although the magnitude of the effect was small relative to the initial treatment. Taking these data together, we conclude that transcription acts in a dynamic manner to regulate the association of a specific set of chromatin and transcriptional regulatory proteins with chromatin.

RNA degradation has similar effects to RNA Pol II inhibition on the interaction of proteins with chromatin

Some of the changes observed upon transcriptional inhibition could reflect the loss of nascent RNA, but others could reflect loss of the process of transcription and its associated histone modifications. That nascent RNA inhibits the association of PRC2 with chromatin is demonstrated by its recruitment to chromatin upon both RNA Pol II inhibition (Riising et al., 2014) and RNaseA treatment (Beltran et al., 2016). Therefore, we considered that the effects of RNA Pol II inhibition due to the loss of nascent RNA should also be observed upon the degradation of RNA in cells with RNaseA. To test this, we permeabilized ESCs and either mock-treated or treated with RNaseA. RNA-seq revealed that this reduced the level of chromatin-associated intronic transcripts by a median of 146-fold, but reduced polyA+ exonic RNA by only 1.3-fold (Figures S2A and S2B). The reason for this differential effect is unclear, but it may represent protection of mature mRNA by ribosomes or other RNA-binding proteins.

We then quantified the change in protein association with the chromatin fraction using label-free LC-MS/MS (Figures 2A and S2C; Table S3). As we had observed upon the inhibition of RNA Pol II, RNA degradation caused the loss of factors involved in RNA processing from chromatin and recruitment of a set of transcriptional and chromatin regulators (Figures 2B; Table S4). Taking the proteins altered by RNA Pol II inhibition and comparing the changes with those caused by RNA degradation revealed a significant correlation (r = 0.45, p = 4.9×10^{-28}, Figures 2C and S2D) and significant overlaps (Figure S2E; 47% of proteins significantly depleted from chromatin after RNA Pol II inhibition were also significantly depleted [FDR < 0.05] from chromatin after RNaseA treatment [p = 83×10^{-45}, hypergeometric]; 24% of proteins significantly enriched on chromatin after RNA Pol II inhibition were also significantly enriched [FDR < 0.05] on chromatin after RNaseA treatment [p = 1.6×10^{-4}]). Immunoblotting demonstrated that the regulatory proteins we had previously confirmed to be recruited to chromatin or depleted from chromatin in response to RNA Pol II inhibition exhibited the same changes in chromatin association upon RNA depletion (Figure 2E).

Not all of the changes in chromatin composition induced by RNA Pol II inhibition were recapitulated by RNA degradation.

(C) Changes in the association of proteins with chromatin upon RNA Pol II inhibition (average of 9-h flavopiridol and triptolide data) and RNA degradation relative to their respective control samples (scale below). Proteins were either recruited to chromatin or depleted from chromatin after both flavopiridol and triptolide treatments. The change in protein chromatin association in response to RNA degradation is shown below and is correlated (r = 0.45, p = 4.9×10^{-28}, n = 527).

(D) Change in chromatin association caused by RNA degradation for the proteins and complexes shown in Figure 1C. Details as for Figure 1C.

(E) Immunoblots for proteins representative of those shown in (D) in the cytoplasmic, nucleoplasmic, and chromatin fractions and WCE purified from ESC after mock treatment (−) or treatment with RNaseA (+).

See also Figure S2 and Tables S3 and S4.

For a minority of factors, RNA degradation had the opposite effect of RNA Pol II inhibition. Rather than being recruited to chromatin, as occurred in response to RNA Pol II inhibition, the THO complex, and Scaffold attachment factor B (SAFB) factors were lost from chromatin upon RNA degradation (Figure 2D), potentially indicating an association with chromatin via stable RNAs. Reciprocally, the PAF complex, which was depleted from chromatin upon RNA Pol II inhibition, was recruited to chromatin upon RNA degradation (Figures S2F and S2G). We conclude that many of the changes in protein chromatin association caused by RNA Pol II inhibition are recapitulated by RNA degradation, suggesting a role for nascent RNA, but that other changes are specific to one of the two treatment types.

RNA antagonizes the interaction of a set of chromatin regulators with nucleosomes

RNA Pol II inhibition and RNA degradation in cells are likely to have pleiotropic effects. Thus, we sought further evidence that RNA inhibited the interaction of chromatin regulatory proteins with chromatin. The antagonistic effect of transcription on the association of PRC2 with chromatin reflects the inhibitory effect of RNA on PRC2 binding to nucleosomes (Beltran et al., 2016, 2019; Wang et al., 2017b). We thus considered that RNA may also antagonize nucleosome binding by the other chromatin regulatory proteins identified in our proteomics analysis. To test this in an unbiased manner, we purified nuclear extract from ESCs, either mock-treated the extract or treated it with RNaseA, incubated the extracts with biotinylated dinucleosomes, purified the nucleosomes with streptavidin beads, and then quantified interacting proteins using SILAC (Figures 3A, S3A, and S3B; Table S5). We identified a set of proteins that exhibited increased binding and a set of proteins that exhibited decreased binding (FDR < 0.05) to nucleosomes after RNA degradation (Figure 3B). Mirroring the effect of RNA Pol II inhibition in cells, the GO term Chromatin Organization was enriched (p = 0.0017; Table S6) in the set of proteins that exhibited increased binding to nucleosomes after RNA degradation. Furthermore, there was a significant overlap between the sets of proteins that exhibited increased binding to nucleosomes after RNA degradation and those that exhibited increased association with chromatin upon RNA Pol II inhibition (26% of proteins enriched on nucleosomes after RNA degradation *in vitro* were also enriched on chromatin after RNA Pol II inhibition in cells; p = 0.027; Figures 3C and S3C). However, differences were also noted. In addition to the chromatin regulators identified in the RNA Pol II inhibition experiment, RNA depletion also increased nucleosome binding by the non-canonical PRC1 complex PRC1.6, the non-specific lethal (NSL) and Ada Two A containing (ATAC) histone acetyltransferase complexes, and the NCOR1, NCOR2, CtBP/LSD1, MiDAC, SIN3A, ING2, and CAF-1 histone deacetylase complexes (Figure 3C), which were either under the significance threshold or were not detected in the cellular chromatin-binding experiments.

To confirm the proteomics results and to distinguish whether RNA inhibited the interaction of the proteins with the core nucleosome particle or with linker DNA, we repeated the experiment with either dinucleosomes, mononucleosomes incorporating linker DNA (185 bp), or mononucleosomes lacking linker DNA (147 bp) and measured changes in nucleosome interaction by immunoblotting (Figures 3D and S3D; Table S5). Of the 16 proteins we tested, 13 were enriched by nucleosome affinity purification, and all of these exhibited increased nucleosome binding upon RNA degradation, including CHD1, CHD4, INO80, EHMT1, SMARCC1, and RUVBL2, thus validating the proteomics data. This experiment also confirmed that RNA antagonized the interaction of PRC2 (SUZ12) with nucleosomes, which did not reach significance (FDR < 0.05) in the proteomics analysis. In contrast, and also consistent with the proteomics data, HMGN1 exhibited decreased binding to nucleosomes upon RNA degradation. Furthermore, these results were apparent for all types of nucleosomes tested, suggesting that RNA modulates the interaction of these factors with the core nucleosome particle rather than with linker DNA. We conclude that nuclear RNA inhibits the association of a set of regulatory proteins with nucleosomes, be this blocking direct interaction with nucleosomes or indirect interaction via a protein partner.

We next considered that if the increase in the binding of these proteins to nucleosomes after RNA degradation reflects the antagonism of nucleosome binding by RNA, then this should be reversed by the re-addition of RNA. Because PRC2 promiscuously binds complex RNAs (Davidovich et al., 2013), tRNA can be used to model the competition between RNA and nucleosomes for PRC2 binding (Beltran et al., 2016). We therefore asked whether the increase in the nucleosome binding of other chromatin regulators upon RNA degradation could also be reversed by the addition of tRNA. To test this, we added tRNA and RNase inhibitor to the RNaseA-treated nuclear extracts and repeated the nucleosome affinity purification and proteomics analysis (Figures 3E and S3E). We found that this generally reversed the changes in nucleosome binding caused by RNA degradation (r = −0.34, p = 3.7 × 10^{-19}), demonstrating that RNA antagonizes the interaction of this set of regulatory proteins with chromatin.

Direct interaction of chromatin regulators with RNA in cells

RNA inhibits the interaction of PRC2 with chromatin because it directly competes with nucleosomes for PRC2 binding (Beltran et al., 2016, 2019; Wang et al., 2017b). Thus, we asked whether the antagonistic effect of RNA on the interaction of regulatory complexes with chromatin could reflect direct interaction between these proteins and RNA. To test this, we selected a set of eight proteins representative of the factors that exhibited increased chromatin binding after RNA degradation: the NuRD component CHD4, the INO80 component INO80, the INO80 and NuA4 component RUVBL2, the BAF components SMARCC1 and SMARCA4, EHMT1, the HMG box transcription factor UBTF, and the integrator subunit INTS11 and used cross-linking and immunoprecipitation (CLIP) to determine whether these proteins directly bound RNA in cells. We detected direct RNA binding for six of these eight proteins in cells (Figures 4A and S4). This was evidenced by the detection of an RNP of the expected molecular weight, with a smear of trimmed RNA extending above, which was stronger in +UV and +PNK (polynucleotide kinase) conditions and which diminished as the RNaseI concentration was increased.

To explore this on a more global scale, we compared the sets of proteins that were depleted or recruited to chromatin
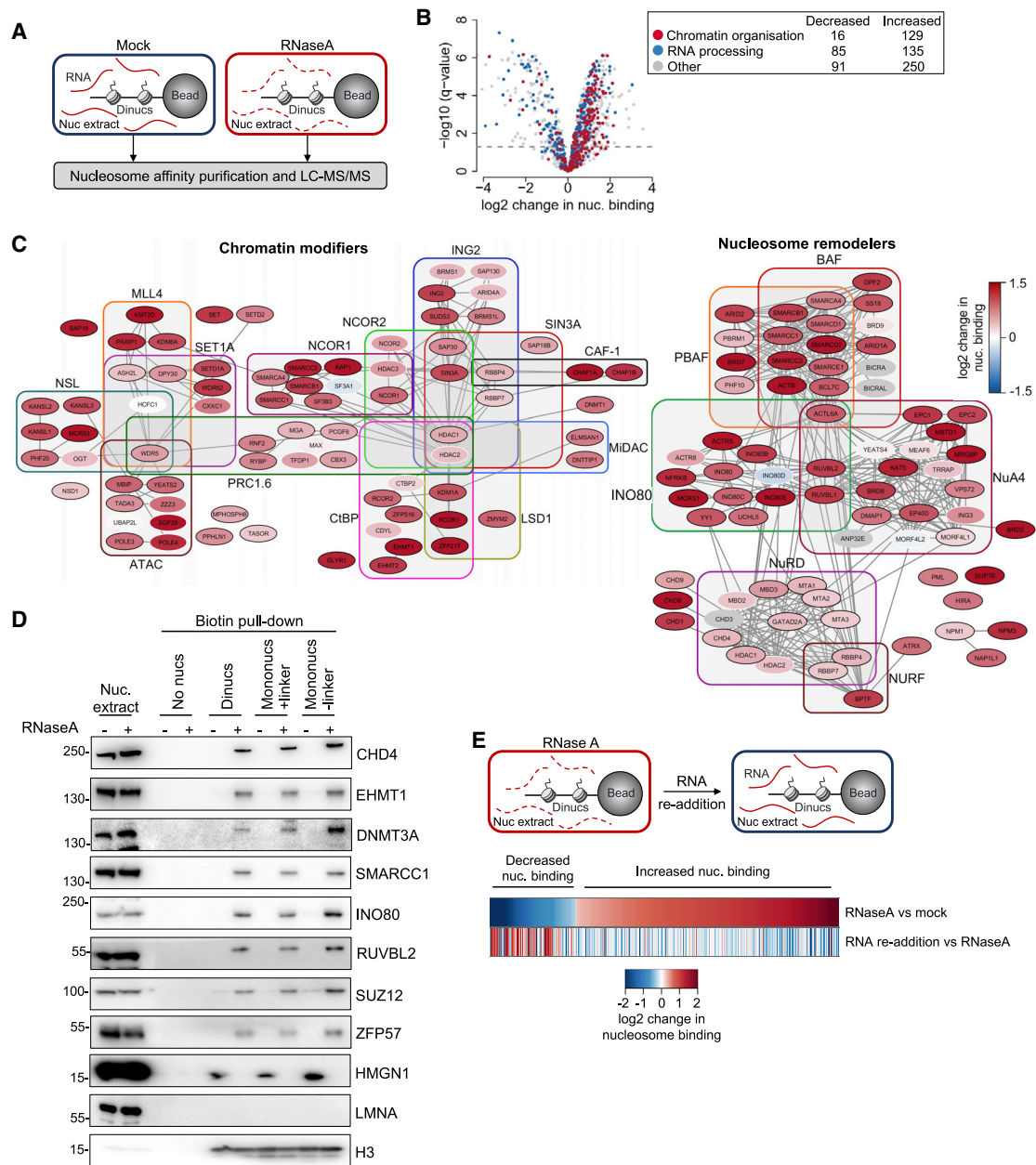
Figure 3. RNA antagonizes the interaction of a set of chromatin regulators with nucleosomes

(A) Experimental strategy. ESC nuclear extract was mock-treated or treated with RNaseA and incubated with biotinylated dinucleosomes, which were then purified by streptavidin affinity purification and bound proteins quantified by SILAC.

(B) Significance of changes in the association of proteins with nucleosomes upon RNaseA treatment versus mock-treated control. Proteins with functions in RNA processing and chromatin organization are highlighted in blue or red, respectively, and their frequencies in the sets of proteins that showed decreased or increased nucleosome binding (FDR < 0.05) shown above.

(C) Chromatin modifiers and nucleosome remodeler complexes that exhibit a significant number of subunits with increased nucleosome binding after degradation of RNA in nuclear extract. Changes in the association of proteins with nucleosomes versus the mock-treated sample are indicated by color, according to the scale on the right, and by the outline (black FDR < 0.05, white FDR > 0.05). Proteins detected in the RNA Pol II inhibition experiment but not this experiment are in gray.

(D) Immunoblots for proteins representative of those shown in (C) in nucleosome pull-downs (dinucleosomes, or mononucleosomes assembled with 187 or 147 bp DNA) from mock-treated (−) or RNaseA-treated (+) nuclear extracts.

(E) Top, strategy: tRNA and RNase inhibitor were added to nuclear extracts after RNaseA-treatment. Bottom: proteins exhibiting either significantly increased or decreased interaction with nucleosomes after RNaseA degradation. Change in nucleosome interaction after tRNA addition is shown below and is anti-correlated ($r = -0.34$, $p = 3.7 \times 10^{-19}$, $n = 668$).

See also Figure S3 and Tables S5 and S6.
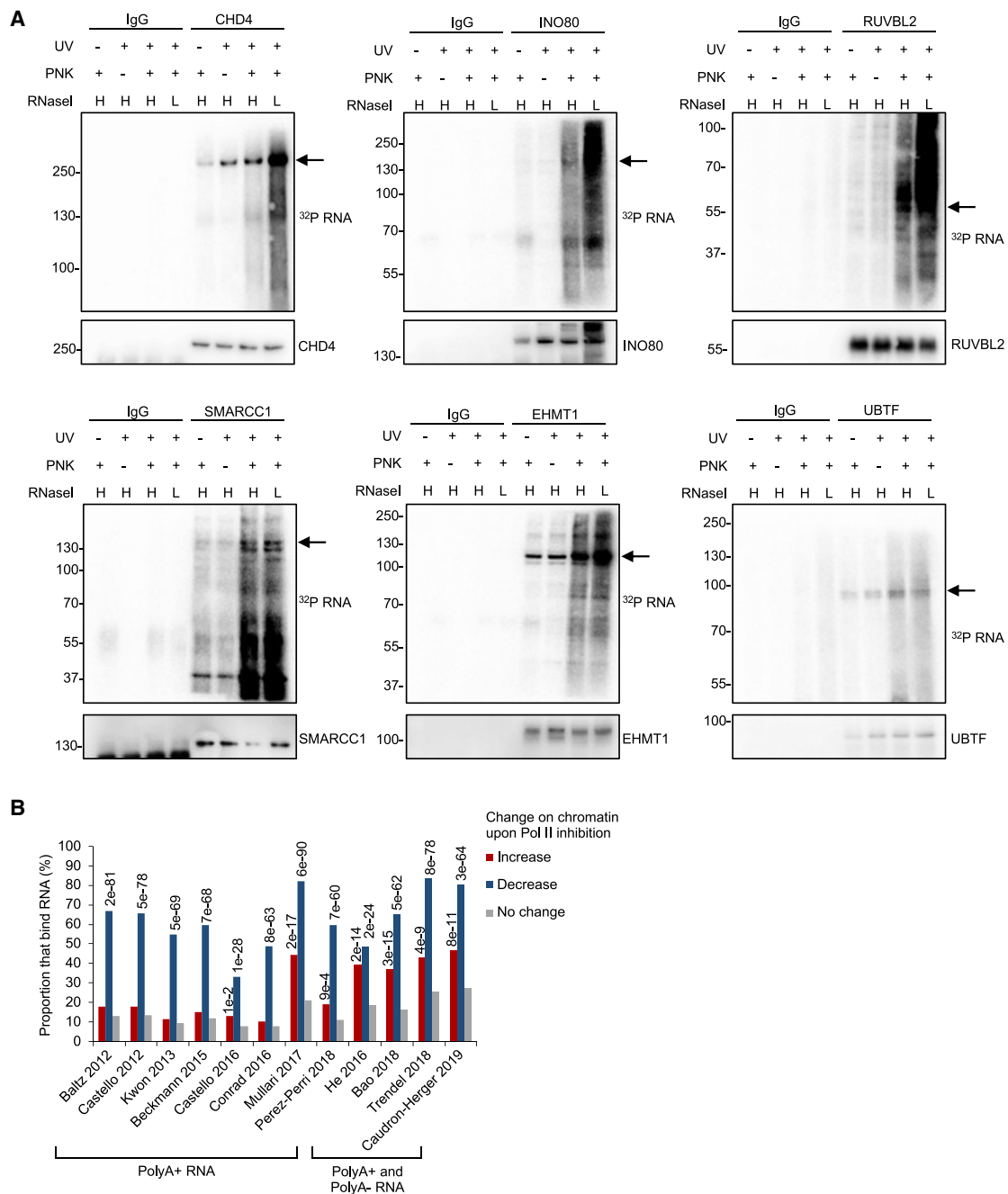
Figure 4. Direct interaction of chromatin regulators with RNA in cells

(A) SDS-PAGE for RNPs enriched by CLIP for CHD4, INO80, RUVBL2, SMARCC1, EHMT1, UBTF, and non-specific immunoglobulin G (IgG) controls in ESCs. Autoradiograms of crosslinked ^{32}P-labeled RNA are shown at the top and the corresponding immunoblots below. CLIP was performed with and without UV crosslinking and polynucleotide kinase (PNK) and with high (H; 40 U/mL) or low (L; 4 U/mL) concentrations of RNase I. The arrows indicate the molecular weight of the protein of interest.

(B) Proportion of proteins exhibiting a significant increase on chromatin (FDR < 0.05, n = 281), decrease on chromatin (FDR < 0.05, n = 241), or no change on chromatin (FDR > 0.05, n = 617) upon treatment with flavopiridol and triptolide (9 h) that were identified as binding RNA in the indicated studies. Studies are divided into those that could only detect binding to polyA+ RNA and those that could also detect binding to non-polyA+ RNA. For each study, significance is estimated relative to the proportion of non-changing proteins identified to bind RNA (binomial test with Bonferroni correction).

See also Figure S4.

upon RNA Pol II inhibition with proteins identified to bind RNA in 12 previous screens, 8 of which identified proteins bound to mature polyadenylated RNA (Baltz et al., 2012; Beckmann et al., 2015; Castello et al., 2012, 2016; Conrad et al., 2016; Kwon et al., 2013; Mullari et al., 2017; Perez-Perri et al., 2018) and 4 of which could also identify proteins bound to nascent RNA or other non-polyadenylated transcripts (Bao et al., 2018; Caudron-Herger et al., 2019; He et al., 2016; Trendel et al., 2019). We found that the set of proteins depleted from chromatin was significantly enriched for RBPs identified by all of the studies (Figure 4B). Then, focusing on the set of proteins recruited to chromatin upon RNA Pol II inhibition, we found that this was significantly enriched for RBPs identified by all four studies that could measure non-polyadenylated RNA binding, including a study that specifically identified proteins bound to nascent RNA (Bao et al., 2018). The set of proteins recruited to chromatin upon RNA Pol II inhibition was also enriched for RBPs identified by three of the eight studies that were limited to polyA+ RNA, albeit to a lesser extent. Together with our CLIP data, these results suggest that the inhibitory effect of RNA on the interaction of these proteins with chromatin is due to the interaction of these factors with RNA.

P-TEFb interacts with nascent pre-mRNA in cells

The P-TEFb subunits CDK9, CyclinT1, and CyclinT2 were among the proteins exhibiting the greatest increases in chromatin association upon RNA Pol II inhibition and RNaseA treatment (Figures 1C and 2D). We hypothesized that the antagonistic effect of RNA on P-TEFb chromatin binding could reflect the interaction of P-TEFb with RNA. Consistent with this possibility, CyclinT1 directly contacts HIV TAR RNA when in a complex with HIV Tat (Garber et al., 1998; Richter et al., 2002; Wei et al., 1998). We tested whether P-TEFb bound to RNA in ESC by performing individual-nucleotide-resolution UV CLIP (iCLIP) for P-TEFb using an antibody specific to CDK9. This resulted in the co-precipitation of CyclinT1 and revealed a UV-dependent RNP that matched the molecular weight of CyclinT1 (Figure S5A). This RNP could also be observed by CLIP with an antibody to CyclinT1 (Figure S5B) and was depleted upon the degradation of CDK9 using THAL-SNS-032, demonstrating it to be dependent on P-TEFb (Figure S5C). We conclude that P-TEFb interacts with RNA in cells. Although the size of the RNP corresponds to CyclinT1, we cannot rule out that other proteins that interact with P-TEFb also contribute to this signal.

Sequencing of P-TEFb RNA crosslink sites revealed strong enrichment for 7SK RNA (Figure S5D), as expected, given its role in sequestering P-TEFb. However, we found that the majority of P-TEFb crosslinks mapped to protein-coding genes with enrichment around 5′ splice sites (5′SS) that was not observed in the background RNA crosslinking from input control samples (Figures 5A and S5E). CLIP for CDK9 did not co-precipitate the 7SK RNP component LARP7 (Figure S5F) and crosslinking around 5′SS was not observed in iCLIP experiments for LARP7 (Figures 5A and S5G), demonstrating that P-TEFb was not binding to pre-mRNA as part of the 7SK RNP. iCLIP for P-TEFb did not enrich for small nuclear RNAs (snRNAs), suggesting that the crosslinking detected around 5′SS does not reflect the co-precipitation of spliceosome components (Figure S5D).

Given the enrichment of P-TEFb RNA crosslinking around 5′SS, we considered that P-TEFb binding to RNA may be dependent on splicing. To test this, we compared P-TEFb crosslinking at 5′SS at exons included in the mature transcript versus exons that were excluded (Figures 5B and S5H). We found that P-TEFb RNA crosslinking was only apparent at included exons, consistent with this crosslinking being dependent on splicing. Furthermore, P-TEFb exhibited reduced crosslinking to RNA transcribed from single-exon compared to multi-exon genes (Figure S5I). To confirm a requirement for splicing, we repeated CDK9 iCLIP after treatment of cells with the SF3b inhibitor pladienolide B (pla-B, 1 μM for 6 h) (Figure 5C). We found that the specific pattern of P-TEFb crosslinking around 5′SS was not observed after treatment with pla-B and conclude that P-TEFb directly binds nascent pre-mRNA around 5′SS and that this is dependent on splicing.

7SK RNA regulates the interaction of P-TEFb with nascent RNA and chromatin

We sought to understand the factors that regulate the interaction of P-TEFb with RNA or chromatin. P-TEFb is held in a poised state by the 7SK RNP, from which it is released to activate transcriptional elongation (Bacon and D'Orso, 2019; Quaresma et al., 2016). The lack of enrichment of the core 7SK RNP component LARP7 with nascent RNA indicated that P-TEFb interacted with nascent RNA in its free, non-7SK associated form. We considered that if this was the case, then the depletion of 7SK RNA should increase P-TEFb binding to nascent RNA. To test this, we performed CLIP for P-TEFb in ESCs transfected with antisense locked nucleic acid (LNA) oligonucleotides specific for 7SK RNA or scrambled control oligos (Figures 6A and S6A). We found that knock down of 7SK increased P-TEFb RNA binding (p = 0.008, Welch's t test), but, in contrast, it had no effect on the binding of LARP7 to RNA. This demonstrates that P-TEFb binds nascent RNA in its free form, and this is countered by its interaction with 7SK.

Given that 7SK antagonized the association of P-TEFb with nascent RNA, we hypothesized that the transfer of P-TEFb to chromatin upon RNA Pol II inhibition may also be regulated by 7SK (transcribed by RNA Pol III). To test this, we measured the effect of RNA Pol II inhibition on the association of P-TEFb with chromatin in WT HAP1 cells and in HAP1 cells in which *7SK* is deleted (Studniarek et al., 2021). We found that treatment with triptolide increased the association of P-TEFb with the chromatin fraction in wild-type (WT) cells but not in 7SK knockout (KO) cells (p < 0.05, Student's t test; Figures 6B and 6C). In contrast, SMARCC1 increased in the chromatin fraction in both WT and 7SK KO cells, while LARP7 showed no change. Thus, 7SK is required for the recruitment of P-TEFb to chromatin upon RNA Pol II inhibition.

The 7SK RNP associates with chromatin at active genes through interaction with KAP1 (McNamara et al., 2016). We therefore considered that the transfer of P-TEFb to chromatin upon RNA Pol II inhibition may depend on KAP1. To test this, we measured the effect of triptolide treatment on P-TEFb chromatin association in WT and KAP1 KO cells. We found that in the absence of KAP1, the extent of P-TEFb recruitment to chromatin was approximately halved (p < 0.05, Student's t test; Figures 6D and 6E), indicating that the association of 7SK with

A

B

C
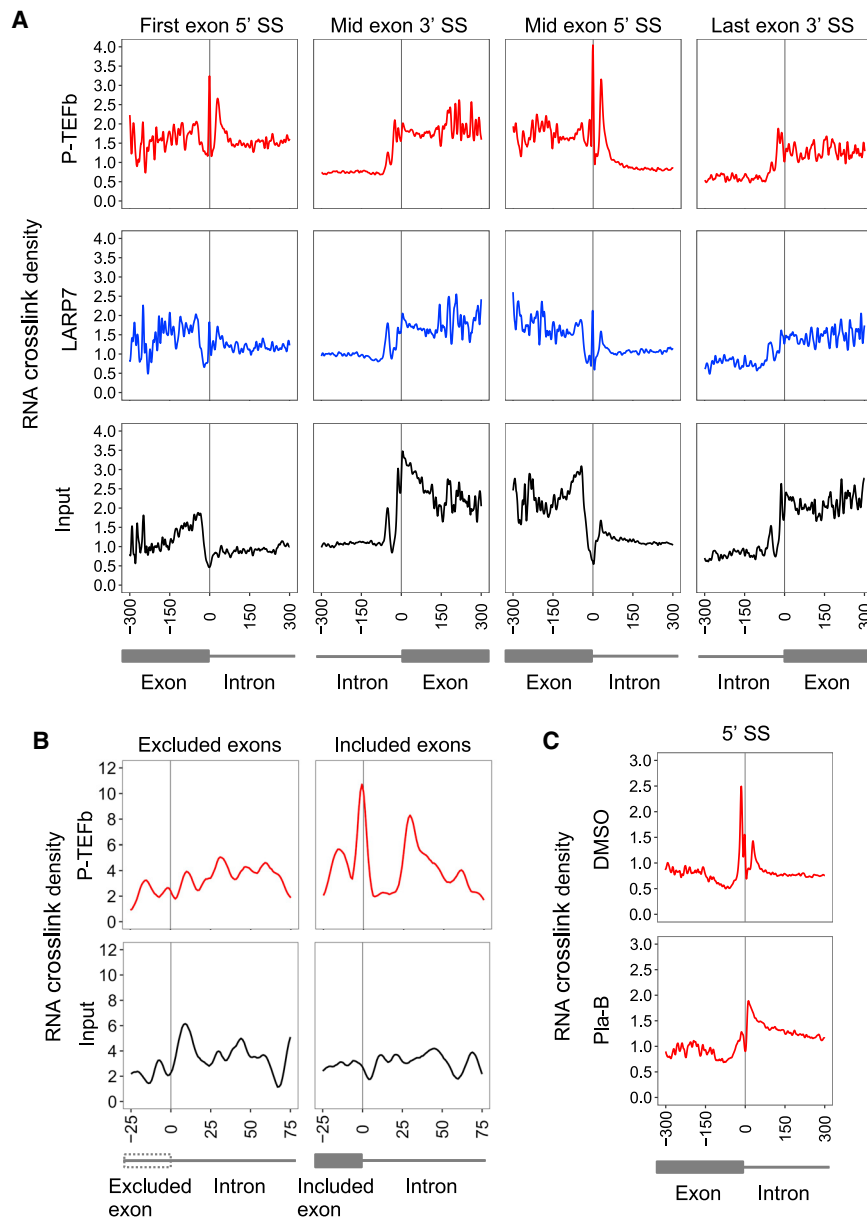
Figure 5. P-TEFb directly interacts with nascent pre-mRNA in cells

(A) Average P-TEFb (red), LARP7 (blue), and background input (black) RNA crosslinking around 5′ splice sites (SS) at first and mid exons and 3′SS at mid and last exons within nascent RNAs at all genes.

(B) Average P-TEFb (red) band background input (black) RNA crosslinking around 5′SS at excluded and included exons.

(C) Average P-TEFb RNA crosslinking at 5′SS in cells treated with DMSO or pladienolide B (pla-B).

See also Figure S5.

DISCUSSION

The antagonistic effect of RNA on the interaction of PRC2 with chromatin has been demonstrated by experiments using RNA Pol II inhibition, RNA degradation, and nucleosome-RNA competition assays (Beltran et al., 2016, 2019; Riising et al., 2014; Wang et al., 2017b). By adapting these methods to allow a more systematic analysis, we have revealed that the antagonistic effect of nascent RNA on PRC2 function is an example of a broader role for RNA in inhibiting the interaction of transcriptional and chromatin regulator proteins with chromatin. That nascent RNA inhibits the association of DNMT1 and DNMT3A with chromatin is consistent with previous data demonstrating that RNA inhibits the activity of these enzymes (Di Ruscio et al., 2013; Hendrickson et al., 2016; Savell et al., 2016), while the identification of BAF is consistent with previous reports that RNA inhibits its interaction with nucleosomes (Cajigas et al., 2015; Han et al., 2014; Jégu et al., 2019; Prensner et al., 2013). That RNA inhibits the interaction of cohesin with chromatin is potentially consistent with previous findings that transcription inhibition induces cohesin accumulation at intragenic sites (Heinz et al., 2018). RNA has not previously been reported to antagonize the interaction of other proteins identified here with chromatin, although a number of the factors have previously been found to bind RNA, including MLL/SET complexes (Wang et al., 2011), BRD4 (Rahnamoun et al., 2018), Integrator (Baillat et al., 2005), INO80 subunits (Davidovic et al., 2006; Jeon and Lee, 2011; Sigova et al., 2015), NuRD (Hendrickson et al., 2016; Zhao et al., 2016), NoRC and CHRAC (Hu et al., 2019; Mayer et al., 2006), cohesin (Hendrickson et al., 2016; Li et al., 2013; Pan et al., 2020; Tsai et al., 2018), CTCF (Hansen et al., 2019; Kung et al., 2015; Saldaña-Meyer et al., 2014), SMCHD1 (Chen et al., 2015), and SAFB (Rivers et al., 2015). The set of proteins identified to be antagonized by RNA is

genes facilitates the recruitment of P-TEFb to chromatin upon RNA Pol II inhibition. We explored whether the requirement for 7SK and KAP1 for the recruitment of P-TEFb to chromatin upon RNA Pol II inhibition was because P-TEFb became associated with 7SK on chromatin. However, CyclinT1 immunoprecipitation from the chromatin fraction revealed a reduction in P-TEFb interaction with 7SK RNA and LARP7 after RNA Pol II inhibition (Figure S6B). Thus, 7SK is necessary for the transfer of P-TEFb to chromatin upon transcriptional inhibition but does not itself constitute the chromatin-associated P-TEFb pool in transcriptionally inactive cells. These data support a model in which nascent RNA binds to a set of transcriptional and chromatin regulators and inhibits their association with chromatin, which, in the case of P-TEFb, is regulated by the 7SK RNP (Figure 6F).

Figure 6. 7SK RNA regulates the interaction of P-TEFb with nascent RNA and chromatin

(A) Left: SDS-PAGE for RNPs enriched by CLIP for P-TEFb and LARP7 in ESCs transfected with scrambled antisense oligonucleotide (ASO) or ASO specific for 7SK RNA. Autoradiograms of crosslinked RNA are shown at the top and immunoblots below. Right: quantification of the change in RNA crosslinking (7SK ASO versus scrambled ASO) relative to protein (means ±SDs, n = 7 [P-TEFb] or n = 2 [LARP7], 1-sided Welch's t test).

(B) Immunoblots for CyclinT1 (CCNT1), CDK9, LARP7, SMARCC1, and control proteins in cytoplasmic, nucleoplasmic, and chromatin fractions and WCE from WT and 7SK KO HAP1 cells after incubation with triptolide for 0, 3, and 6 h.

(C) Quantification of immunoblots shown in (B), measuring chromatin association of each protein relative to t = 0 (means ± SDs, 1-sided Student's t test, 4 independent experiments).

(D) Immunoblots in cytoplasmic, nucleoplasmic, and chromatin fractions and WCE from WT and KAP1 KO HEK293T cells after incubation with triptolide for 0, 3, and 6 h.

(E) Quantification of immunoblots shown in (E), measuring chromatin association of each protein relative to t = 0 (means ± SDs, 1-sided Student's t test, 3 independent experiments).

(F) Model: nascent RNA binds a set of transcriptional and chromatin regulators and antagonizes their association with chromatin. For some of these factors, RNA inhibits their interaction with nucleosomes. For P-TEFb, RNA binding and recruitment to chromatin are regulated by the 7SK RNP.

See also Figure S6.

enriched for functions in ESC pluripotency, and a number of the factors share subunits and/or function together in common pathways—for example, PRC2 with NuRD (Reynolds et al., 2012) and INO80 (Xue et al., 2017)—suggesting that nascent RNA regulates the interaction of factors with chromatin in a coordinated manner.

Of the factors we identified to be regulated by nascent RNA, we focused on P-TEFb because its subunits were among the proteins exhibiting the greatest increases in chromatin association upon RNA Pol II inhibition and because it had previously been shown to directly bind HIV TAR RNA (Garber et al., 1998; Richter et al., 2002). The RNA Pol II Ser-2 kinases Ctk1 and Bur1 have also been found to directly bind nascent RNA in *Saccharomyces cerevisiae*, suggesting that nascent RNA binding activity is conserved in eukaryotes (Battaglia et al., 2017). However, in yeast, RNaseA treatment reduced rather than increased the association of Ctk1 and Bur1 with chromatin (Battaglia et al., 2017), potentially reflecting differences in the mechanisms of chromatin association between species.

Our discovery that nascent pre-mRNA interacts with P-TEFb and antagonizes its association with chromatin suggests that cellular pre-mRNA may act in a manner analogous to that of TAR, which releases the Tat:P-TEFb complex from the 7SK RNP (D'Orso and Frankel, 2010). The RNA-binding proteins SRSF2 (Ji et al., 2013), DDX21 (Calo et al., 2015), WDR43 (Bi et al., 2019), and RBM7 (Bugai et al., 2019) have been found to release P-TEFb from 7SK and increase RNA Pol II Ser-2P, and thus may act in a manner analogous to that of Tat. In particular, SRSF2 both promotes splicing and P-TEFb recruitment to genes (Ji et al., 2013; Lin et al., 2008), which is potentially consistent with the requirement for splicing for P-TEFb binding to 5′SS.

Further studies will be required to ascertain the importance of nascent RNA binding for P-TEFb function. Interaction of P-TEFb with nascent pre-mRNA could increase the size of the free P-TEFb pool or could specifically direct its activities to particular locations or substrates. For example, P-TEFb binding to internal sites within pre-mRNA could function to maintain Ser-2P as RNA Pol II travels through the gene body. More specifically, the splicing-dependent enrichment of P-TEFb at 5′SS may help couple splicing with transcriptional elongation (Herzel et al., 2017) and may contribute to previously observed stimulatory effects of splicing on Ser-2P and transcriptional elongation (Caizzi et al., 2021; Chathoth et al., 2014; Fong and Zhou, 2001; Ji et al., 2013; Koga et al., 2015; Lin et al., 2008).

Limitations of the study

We recognize that RNA Pol II inhibition and RNA degradation likely have pleiotropic effects on the cell, and thus we sought to identify changes in protein chromatin association that were common to both treatments and also complemented these cellular treatments with measurement of the effect of RNA depletion from nuclear extracts on the interaction of proteins with nucleosomes. RNA Pol II inhibition and RNA degradation had a greater effect on nascent transcripts than on mature polyA+ RNA species, suggesting that changes in the interaction of proteins with chromatin are primarily due to the loss of nascent RNA, but it is possible that some of the effects are caused by the loss of short-lived mature RNAs. The experimental design also does not distinguish between the effects of pre-mRNAs versus other nascent RNA species. However, it is likely that much of the effect is due to pre-mRNAs because these represent the majority of nascent and chromatin-associated RNAs in the cell (Mondal et al., 2010; Nozawa and Gilbert, 2019; St Laurent et al., 2012) and, where known, the majority of RNAs bound by the factors identified here, including PRC2 (Beltran et al., 2016), DNMT1 (Hendrickson et al., 2016), DNMT3A (Savell et al., 2016), the NuRD components CHD4 and HDAC1 (Hendrickson et al., 2016), and P-TEFb (this study). Further work will be necessary to determine the RNA species bound by the factors identified, the binding sites on chromatin affected by RNA, and the importance of RNA binding activity for the function of the proteins in the cell. In the case of P-TEFb, further work is necessary to identify the factor(s) that mediate its association with chromatin upon RNA Pol II inhibition.

In summary, our work demonstrates that nascent RNA regulates the interaction of a set of chromatin and transcriptional regulatory factors with chromatin and primarily acts to antagonize their interaction with chromatin. These results are consistent with models in which nascent RNA provides direct feedback from gene transcription to chromatin state (Skalska et al., 2017) and provides evidence of a close interplay between RNA and chromatin in gene regulation. Nascent RNAs and other transcripts have been proposed to contribute to a dynamic matrix or phase-separated compartments that regulate chromatin state (Hnisz et al., 2017; Nozawa and Gilbert, 2019). Thus, these structures may function in part by concentrating the antagonistic effects of RNA at regions of active chromatin in the cell.

STAR★METHODS

Detailed methods are provided in the online version of this paper and include the following:

- **KEY RESOURCES TABLE**
- **RESOURCE AVAILABILITY**
  - Lead contact
  - Materials availability
  - Data and code availability
- **EXPERIMENTAL MODEL AND SUBJECT DETAILS**
- **METHOD DETAILS**
  - Cell fractionation for proteomics experiments
  - Nucleosome affinity purification for proteomics
  - SILAC
  - Label-free quantification (LFQ)
  - Cell fractionation for validation experiments
  - Nucleosome affinity purification validation
  - Immunoblotting
  - 7SK knockdown
  - CLIP
  - iCLIP
  - Co-immunoprecipitation from chromatin
  - RNA-seq
  - Cell cycle, caspase activation, cell death, γH2A.X
- **QUANTIFICATION AND STATISTICAL ANALYSIS**
  - Mass-spectrometry data analysis
  - LC-MS/MS data post-processing and analysis

- ○ iCLIP data analysis
- ○ RNA-seq analysis
- ○ Comparison to RNA binding studies
- ○ CLIP and immunoblotting

SUPPLEMENTAL INFORMATION

Supplemental information can be found online at https://doi.org/10.1016/j.molcel.2021.05.026.

AUTHOR CONTRIBUTIONS

Conceptualization, L.S., M.B., and R.G.J.; methodology, L.S., M.B., and R.G.J.; software, S.L. and G.K.; validation, L.S., V.B., M.B., and R.W.; formal analysis, V.B., S.L., G.K., P.F., S.S., and R.G.J.; investigation, L.S., M.B., V.B., P.F., A.B., M.T., and R.W.; resources, L.S., A.T., B.M.F., J.H., and A.P.S.; data curation, V.B., S.L., G.K., P.F., I.R.D.L.M., S.S., and R.G.J.; writing – original draft, R.G.J.; writing – review & editing, L.S., V.B., M.B., S.L., T.B., and R.G.J.; visualization, L.S., V.B., M.B., S.L., G.K., M.T., and R.G.J.; supervision, J.H., S.S., A.P.S., T.B., and R.G.J.

DECLARATION OF INTERESTS

The authors declare no competing interests.

REFERENCES

Bacon, C.W., and D'Orso, I. (2019). CDK9: a signaling hub for transcriptional control. Transcription 10, 57–75.

Baillat, D., Hakimi, M.A., Näär, A.M., Shilatifard, A., Cooch, N., and Shiekhattar, R. (2005). Integrator, a multiprotein mediator of small nuclear RNA processing, associates with the C-terminal repeat of RNA polymerase II. Cell 123, 265–276.

Baltz, A.G., Munschauer, M., Schwanhäusser, B., Vasile, A., Murakawa, Y., Schueler, M., Youngs, N., Penfold-Brown, D., Drew, K., Milek, M., et al. (2012). The mRNA-bound proteome and its global occupancy profile on protein-coding transcripts. Mol. Cell 46, 674–690.

Bao, X., Guo, X., Yin, M., Tariq, M., Lai, Y., Kanwal, S., Zhou, J., Li, N., Lv, Y., Pulido-Quetglas, C., et al. (2018). Capturing the interactome of newly transcribed RNA. Nat. Methods 15, 213–220.

Barboric, M., Yik, J.H., Czudnochowski, N., Yang, Z., Chen, R., Contreras, X., Geyer, M., Matija Peterlin, B., and Zhou, Q. (2007). Tat competes with HEXIM1 to increase the active pool of P-TEFb for HIV-1 transcription. Nucleic Acids Res. 35, 2003–2012.

Barutcu, A.R., Blencowe, B.J., and Rinn, J.L. (2019). Differential contribution of steady-state RNA and active transcription in chromatin organization. EMBO Rep. 20, e48068.

Battaglia, S., Lidschreiber, M., Baejen, C., Torkler, P., Vos, S.M., and Cramer, P. (2017). RNA-dependent chromatin association of transcription elongation factors and Pol II CTD kinases. eLife 6, e25637.

Beckmann, B.M., Horos, R., Fischer, B., Castello, A., Eichelbaum, K., Alleaume, A.M., Schwarzl, T., Curk, T., Foehr, S., Huber, W., et al. (2015). The RNA-binding proteomes from yeast to man harbour conserved enigmRBPs. Nat. Commun. 6, 10127.

Beltran, M., Yates, C.M., Skalska, L., Dawson, M., Reis, F.P., Viiri, K., Fisher, C.L., Sibley, C.R., Foster, B.M., Bartke, T., et al. (2016). The interaction of PRC2 with RNA or chromatin is mutually antagonistic. Genome Res. 26, 896–907.

Beltran, M., Tavares, M., Justin, N., Khandelwal, G., Ambrose, J., Foster, B.M., Worlock, K.B., Tvardovskiy, A., Kunzelmann, S., Herrero, J., et al. (2019). G-tract RNA removes Polycomb repressive complex 2 from genes. Nat. Struct. Mol. Biol. 26, 899–909.

Bi, X., Xu, Y., Li, T., Li, X., Li, W., Shao, W., Wang, K., Zhan, G., Wu, Z., Liu, W., et al. (2019). RNA Targets Ribogenesis Factor WDR43 to Chromatin for Transcription and Pluripotency Control. Mol. Cell 75, 102–116.e9.

Bugai, A., Quaresma, A.J.C., Friedel, C.C., Lenasi, T., Düster, R., Sibley, C.R., Fujinaga, K., Kukanja, P., Hennig, T., Blasius, M., et al. (2019). P-TEFb Activation by RBM7 Shapes a Pro-survival Transcriptional Response to Genotoxic Stress. Mol. Cell 74, 254–267.e10.

Caizzi, L., Monteiro-Martins, S., Schwalb, B., Lysakovskaia, K., Schmitzova, J., Sawicka, A., Chen, Y., Lidschreiber, M., and Cramer, P. (2021). Efficient RNA polymerase II pause release requires U2 snRNP function. Mol. Cell 81, 1920–1934.e9.

Cajigas, I., Leib, D.E., Cochrane, J., Luo, H., Swyter, K.R., Chen, S., Clark, B.S., Thompson, J., Yates, J.R., 3rd, Kingston, R.E., and Kohtz, J.D. (2015). Evf2 lncRNA/BRG1/DLX1 interactions reveal RNA-dependent inhibition of chromatin remodeling. Development 142, 2641–2652.

Calo, E., Flynn, R.A., Martin, L., Spitale, R.C., Chang, H.Y., and Wysocka, J. (2015). RNA helicase DDX21 coordinates transcription and ribosomal RNA processing. Nature 518, 249–253.

Castello, A., Fischer, B., Eichelbaum, K., Horos, R., Beckmann, B.M., Strein, C., Davey, N.E., Humphreys, D.T., Preiss, T., Steinmetz, L.M., et al. (2012). Insights into RNA biology from an atlas of mammalian mRNA-binding proteins. Cell 149, 1393–1406.

Castello, A., Fischer, B., Frese, C.K., Horos, R., Alleaume, A.M., Foehr, S., Curk, T., Krijgsveld, J., and Hentze, M.W. (2016). Comprehensive Identification of RNA-Binding Domains in Human Cells. Mol. Cell 63, 696–710.

Caudron-Herger, M., Rusin, S.F., Adamo, M.E., Seiler, J., Schmid, V.K., Barreau, E., Kettenbach, A.N., and Diederichs, S. (2019). R-DeeP: Proteome-wide and Quantitative Identification of RNA-Dependent Proteins by Density Gradient Ultracentrifugation. Mol. Cell 75, 184–199.e10.

Chathoth, K.T., Barrass, J.D., Webb, S., and Beggs, J.D. (2014). A splicing-dependent transcriptional checkpoint associated with prespliceosome formation. Mol. Cell 53, 779–790.

Chen, K., Hu, J., Moore, D.L., Liu, R., Kessans, S.A., Breslin, K., Lucet, I.S., Keniry, A., Leong, H.S., Parish, C.L., et al. (2015). Genome-wide binding and mechanistic analyses of Smchd1-mediated epigenetic regulation. Proc. Natl. Acad. Sci. USA 112, E3535–E3544.

Cifuentes-Rojas, C., Hernandez, A.J., Sarma, K., and Lee, J.T. (2014). Regulatory interactions between RNA and polycomb repressive complex 2. Mol. Cell 55, 171–185.

Conrad, T., Albrecht, A.S., de Melo Costa, V.R., Sauer, S., Meierhofer, D., and Ørom, U.A. (2016). Serial interactome capture of the human cell nucleus. Nat. Commun. 7, 11212.

Cox, J., and Mann, M. (2008). MaxQuant enables high peptide identification rates, individualized p.p.b.-range mass accuracies and proteome-wide protein quantification. Nat. Biotechnol. 26, 1367–1372.

D'Orso, I., and Frankel, A.D. (2010). RNA-mediated displacement of an inhibitory snRNP complex activates transcription elongation. Nat. Struct. Mol. Biol. *17*, 815–821.

Davidovic, L., Bechara, E., Gravel, M., Jaglin, X.H., Tremblay, S., Sik, A., Bardoni, B., and Khandjian, E.W. (2006). The nuclear microspherule protein 58 is a novel RNA-binding protein that interacts with fragile X mental retardation protein in polyribosomal mRNPs from neurons. Hum. Mol. Genet. *15*, 1525–1538.

Davidovich, C., Zheng, L., Goodrich, K.J., and Cech, T.R. (2013). Promiscuous RNA binding by Polycomb repressive complex 2. Nat. Struct. Mol. Biol. *20*, 1250–1257.

Di Ruscio, A., Ebralidze, A.K., Benoukraf, T., Amabile, G., Goff, L.A., Terragni, J., Figueroa, M.E., De Figueiredo Pontes, L.L., Alberich-Jorda, M., Zhang, P., et al. (2013). DNMT1-interacting RNAs block gene-specific DNA methylation. Nature *503*, 371–376.

Dobin, A., Davis, C.A., Schlesinger, F., Drenkow, J., Zaleski, C., Jha, S., Batut, P., Chaisson, M., and Gingeras, T.R. (2013). STAR: ultrafast universal RNA-seq aligner. Bioinformatics *29*, 15–21.

Flynn, R.A., Do, B.T., Rubin, A.J., Calo, E., Lee, B., Kuchelmeister, H., Rale, M., Chu, C., Kool, E.T., Wysocka, J., et al. (2016). 7SK-BAF axis controls pervasive transcription at enhancers. Nat. Struct. Mol. Biol. *23*, 231–238.

Fong, Y.W., and Zhou, Q. (2001). Stimulatory effect of splicing factors on transcriptional elongation. Nature *414*, 929–933.

Hendrickson, D.G., Kelley, D.R., Tenen, D., Bernstein, B., and Rinn, J.L. (2016). Widespread RNA binding by chromatin-associated proteins. Genome Biol. *17*, 28.

Garber, M.E., Wei, P., KewalRamani, V.N., Mayall, T.P., Herrmann, C.H., Rice, A.P., Littman, D.R., and Jones, K.A. (1998). The interaction between HIV-1 Tat and human cyclin T1 requires zinc and a critical cysteine residue that is not conserved in the murine CycT1 protein. Genes Dev. *12*, 3512–3527.

Garland, W., Comet, I., Wu, M., Radzisheuskaya, A., Rib, L., Vitting-Seerup, K., Lloret-Llinares, M., Sandelin, A., Helin, K., and Jensen, T.H. (2019). A Functional Link between Nuclear RNA Decay and Transcriptional Control Mediated by the Polycomb Repressive Complex 2. Cell Rep. *29*, 1800–1811.e6.

Giurgiu, M., Reinhard, J., Brauner, B., Dunger-Kaltenbach, I., Fobo, G., Frishman, G., Montrone, C., and Ruepp, A. (2019). CORUM: the comprehensive resource of mammalian protein complexes-2019. Nucleic Acids Res. *47* (D1), D559–D563.

Han, P., Li, W., Lin, C.H., Yang, J., Shang, C., Nuernberg, S.T., Jin, K.K., Xu, W., Lin, C.Y., Lin, C.J., et al. (2014). A long noncoding RNA protects the heart from pathological hypertrophy. Nature *514*, 102–106.

Hansen, A.S., Hsieh, T.S., Cattoglio, C., Pustova, I., Saldaña-Meyer, R., Reinberg, D., Darzacq, X., and Tjian, R. (2019). Distinct Classes of Chromatin Loops Revealed by Deletion of an RNA-Binding Region in CTCF. Mol. Cell *76*, 395–411.e13.

He, C., Sidoli, S., Warneford-Thomson, R., Tatomer, D.C., Wilusz, J.E., Garcia, B.A., and Bonasio, R. (2016). High-Resolution Mapping of RNA-Binding Regions in the Nuclear Proteome of Embryonic Stem Cells. Mol. Cell *64*, 416–430.

Heinz, S., Texari, L., Hayes, M.G.B., Urbanowski, M., Chang, M.W., Givarkes, N., Rialdi, A., White, K.M., Albrecht, R.A., Pache, L., et al. (2018). Transcription Elongation Can Affect Genome 3D Structure. Cell *174*, 1522–1536.e22.

Herzel, L., Ottoz, D.S.M., Alpert, T., and Neugebauer, K.M. (2017). Splicing and transcription touch base: co-transcriptional spliceosome assembly and function. Nat. Rev. Mol. Cell Biol. *18*, 637–650.

Herzog, V.A., Lempradl, A., Trupke, J., Okulski, H., Altmutter, C., Ruge, F., Boidol, B., Kubicek, S., Schmauss, G., Aumayr, K., et al. (2014). A strand-specific switch in noncoding transcription switches the function of a Polycomb/Trithorax response element. Nat. Genet. *46*, 973–981.

Hnisz, D., Shrinivas, K., Young, R.A., Chakraborty, A.K., and Sharp, P.A. (2017). A Phase Separation Model for Transcriptional Control. Cell *169*, 13–23.

Hooper, M., Hardy, K., Handyside, A., Hunter, S., and Monk, M. (1987). HPRT-deficient (Lesch-Nyhan) mouse embryos derived from germline colonization by cultured cells. Nature *326*, 292–295.

Hosogane, M., Funayama, R., Shirota, M., and Nakayama, K. (2016). Lack of Transcription Triggers H3K27me3 Accumulation in the Gene Body. Cell Rep. *16*, 696–706.

Hu, Y.W., Guo, F.X., Xu, Y.J., Li, P., Lu, Z.F., McVey, D.G., Zheng, L., Wang, Q., Ye, J.H., Kang, C.M., et al. (2019). Long noncoding RNA NEXN-AS1 mitigates atherosclerosis by regulating the actin-binding protein NEXN. J. Clin. Invest. *129*, 1115–1128.

Huppertz, I., Attig, J., D'Ambrogio, A., Easton, L.E., Sibley, C.R., Sugimoto, Y., Tajnik, M., König, J., and Ule, J. (2014). iCLIP: protein-RNA interactions at nucleotide resolution. Methods *65*, 274–287.

Jégu, T., Blum, R., Cochrane, J.C., Yang, L., Wang, C.Y., Gilles, M.E., Colognori, D., Szanto, A., Marr, S.K., Kingston, R.E., and Lee, J.T. (2019). Xist RNA antagonizes the SWI/SNF chromatin remodeler BRG1 on the inactive X chromosome. Nat. Struct. Mol. Biol. *26*, 96–109.

Jeon, Y., and Lee, J.T. (2011). YY1 tethers Xist RNA to the inactive X nucleation center. Cell *146*, 119–133.

Ji, X., Zhou, Y., Pandit, S., Huang, J., Li, H., Lin, C.Y., Xiao, R., Burge, C.B., and Fu, X.D. (2013). SR proteins collaborate with 7SK and promoter-associated nascent RNA to release paused polymerase. Cell *153*, 855–868.

Kammers, K., Cole, R.N., Tiengwe, C., and Ruczinski, I. (2015). Detecting Significant Changes in Protein Abundance. EuPA Open Proteom. *7*, 11–19.

Kaneko, S., Son, J., Shen, S.S., Reinberg, D., and Bonasio, R. (2013). PRC2 binds active promoters and contacts nascent RNAs in embryonic stem cells. Nat. Struct. Mol. Biol. *20*, 1258–1264.

Kaneko, S., Son, J., Bonasio, R., Shen, S.S., and Reinberg, D. (2014). Nascent RNA interaction keeps PRC2 activity poised and in check. Genes Dev. *28*, 1983–1988.

Kanhere, A., Viiri, K., Araújo, C.C., Rasaiyaah, J., Bouwman, R.D., Whyte, W.A., Pereira, C.F., Brookes, E., Walker, K., Bell, G.W., et al. (2010). Short RNAs are transcribed from repressed polycomb target genes and interact with polycomb repressive complex-2. Mol. Cell *38*, 675–688.

Katz, Y., Wang, E.T., Airoldi, E.M., and Burge, C.B. (2010). Analysis and design of RNA sequencing experiments for identifying isoform regulation. Nat. Methods *7*, 1009–1015.

Koga, M., Hayashi, M., and Kaida, D. (2015). Splicing inhibition decreases phosphorylation level of Ser2 in Pol II CTD. Nucleic Acids Res. *43*, 8258–8267.

König, J., Zarnack, K., Rot, G., Curk, T., Kayikci, M., Zupan, B., Turner, D.J., Luscombe, N.M., and Ule, J. (2010). iCLIP reveals the function of hnRNP particles in splicing at individual nucleotide resolution. Nat. Struct. Mol. Biol. *17*, 909–915.

Kung, J.T., Kesner, B., An, J.Y., Ahn, J.Y., Cifuentes-Rojas, C., Colognori, D., Jeon, Y., Szanto, A., del Rosario, B.C., Pinter, S.F., et al. (2015). Locus-specific targeting to the X chromosome revealed by the RNA interactome of CTCF. Mol. Cell *57*, 361–375.

Kwon, S.C., Yi, H., Eichelbaum, K., Föhr, S., Fischer, B., You, K.T., Castello, A., Krijgsveld, J., Hentze, M.W., and Kim, V.N. (2013). The RNA-binding protein repertoire of embryonic stem cells. Nat. Struct. Mol. Biol. *20*, 1122–1130.

Langmead, B., and Salzberg, S.L. (2012). Fast gapped-read alignment with Bowtie 2. Nat. Methods *9*, 357–359.

Li, W., Notani, D., Ma, Q., Tanasa, B., Nunez, E., Chen, A.Y., Merkurjev, D., Zhang, J., Ohgi, K., Song, X., et al. (2013). Functional roles of enhancer RNAs for oestrogen-dependent transcriptional activation. Nature *498*, 516–520.

Li, L., Lyu, X., Hou, C., Takenaka, N., Nguyen, H.Q., Ong, C.T., Cubeñas-Potts, C., Hu, M., Lei, E.P., Bosco, G., et al. (2015). Widespread rearrangement of 3D chromatin organization underlies polycomb-mediated stress-induced silencing. Mol. Cell *58*, 216–231.

Liao, Y., Smyth, G.K., and Shi, W. (2014). featureCounts: an efficient general purpose program for assigning sequence reads to genomic features. Bioinformatics *30*, 923–930.

Lin, S., Coutinho-Mansfield, G., Wang, D., Pandit, S., and Fu, X.D. (2008). The splicing factor SC35 has an active role in transcriptional elongation. Nat. Struct. Mol. Biol. *15*, 819–826.

Love, M.I., Huber, W., and Anders, S. (2014). Moderated estimation of fold change and dispersion for RNA-seq data with DESeq2. Genome Biol. *15*, 550.

Makowski, M.M., Gräwe, C., Foster, B.M., Nguyen, N.V., Bartke, T., and Vermeulen, M. (2018). Global profiling of protein-DNA and protein-nucleosome binding affinities using quantitative mass spectrometry. Nat. Commun. *9*, 1653.

Mayer, C., Schmitz, K.M., Li, J., Grummt, I., and Santoro, R. (2006). Intergenic transcripts regulate the epigenetic state of rRNA genes. Mol. Cell *22*, 351–361.

McNamara, R.P., Reeder, J.E., McMillan, E.A., Bacon, C.W., McCann, J.L., and D'Orso, I. (2016). KAP1 Recruitment of the 7SK snRNP Complex to Promoters Enables Transcription Elongation by RNA Polymerase II. Mol. Cell *61*, 39–53.

Michels, A.A., Nguyen, V.T., Fraldi, A., Labas, V., Edwards, M., Bonnet, F., Lania, L., and Bensaude, O. (2003). MAQ1 and 7SK RNA interact with CDK9/cyclin T complexes in a transcription-dependent manner. Mol. Cell. Biol. *23*, 4859–4869.

Mondal, T., Rasmussen, M., Pandey, G.K., Isaksson, A., and Kanduri, C. (2010). Characterization of the RNA content of chromatin. Genome Res. *20*, 899–907.

Monte, E., Chen, H., Kolmakova, M., Parvatiyar, M., Vondriska, T.M., and Franklin, S. (2012). Quantitative analysis of chromatin proteomes in disease. J. Vis. Exp. *70*, 4294.

Mullari, M., Lyon, D., Jensen, L.J., and Nielsen, M.L. (2017). Specifying RNA-Binding Regions in Proteins by Peptide Cross-Linking and Affinity Purification. J. Proteome Res. *16*, 2762–2772.

Nickerson, J.A., Krochmalnic, G., Wan, K.M., and Penman, S. (1989). Chromatin architecture and nuclear RNA. Proc. Natl. Acad. Sci. USA *86*, 177–181.

Nozawa, R.S., and Gilbert, N. (2019). RNA: Nuclear Glue for Folding the Genome. Trends Cell Biol. *29*, 201–211.

Nozawa, R.S., Boteva, L., Soares, D.C., Naughton, C., Dun, A.R., Buckle, A., Ramsahoye, B., Bruton, P.C., Saleeb, R.S., Arnedo, M., et al. (2017). SAF-A Regulates Interphase Chromosome Structure through Oligomerization with Chromatin-Associated RNAs. Cell *169*, 1214–1227.e18.

Pan, H., Jin, M., Ghadiyaram, A., Kaur, P., Miller, H.E., Ta, H.M., Liu, M., Fan, Y., Mahn, C., Gorthi, A., et al. (2020). Cohesin SA1 and SA2 are RNA binding proteins that localize to RNA containing regions on DNA. Nucleic Acids Res. *48*, 5639–5655.

Perez-Perri, J.I., Rogell, B., Schwarzl, T., Stein, F., Zhou, Y., Rettel, M., Brosig, A., and Hentze, M.W. (2018). Discovery of RNA-binding proteins and characterization of their dynamic responses by enhanced RNA interactome capture. Nat. Commun. *9*, 4408.

Perez-Riverol, Y., Csordas, A., Bai, J., Bernal-Llinares, M., Hewapathirana, S., Kundu, D.J., Inuganti, A., Griss, J., Mayer, G., Eisenacher, M., et al. (2019). The PRIDE database and related tools and resources in 2019: improving support for quantification data. Nucleic Acids Res. *47* (D1), D442–D450.

Prensner, J.R., Iyer, M.K., Sahu, A., Asangani, I.A., Cao, Q., Patel, L., Vergara, I.A., Davicioni, E., Erho, N., Ghadessi, M., et al. (2013). The long noncoding RNA SChLAP1 promotes aggressive prostate cancer and antagonizes the SWI/SNF complex. Nat. Genet. *45*, 1392–1398.

Quaresma, A.J.C., Bugai, A., and Barboric, M. (2016). Cracking the control of RNA polymerase II elongation by 7SK snRNP and P-TEFb. Nucleic Acids Res. *44*, 7527–7539.

Rahnamoun, H., Lee, J., Sun, Z., Lu, H., Ramsey, K.M., Komives, E.A., and Lauberth, S.M. (2018). RNAs interact with BRD4 to promote enhanced chromatin engagement and transcription activation. Nat. Struct. Mol. Biol. *25*, 687–697.

Ramírez, F., Ryan, D.P., Grüning, B., Bhardwaj, V., Kilpert, F., Richter, A.S., Heyne, S., Dündar, F., and Manke, T. (2016). deepTools2: a next generation web server for deep-sequencing data analysis. Nucleic Acids Res. *44* (W1), W160–W165.

Raudvere, U., Kolberg, L., Kuzmin, I., Arak, T., Adler, P., Peterson, H., and Vilo, J. (2019). g:Profiler: a web server for functional enrichment analysis and conversions of gene lists (2019 update). Nucleic Acids Res. *47* (W1), W191–W198.

Reynolds, N., Salmon-Divon, M., Dvinge, H., Hynes-Allen, A., Balasooriya, G., Leaford, D., Behrens, A., Bertone, P., and Hendrich, B. (2012). NuRD-mediated deacetylation of H3K27 facilitates recruitment of Polycomb Repressive Complex 2 to direct gene repression. EMBO J. *31*, 593–605.

Richter, S., Ping, Y.H., and Rana, T.M. (2002). TAR RNA loop: a scaffold for the assembly of a regulatory switch in HIV replication. Proc. Natl. Acad. Sci. USA *99*, 7928–7933.

Riising, E.M., Comet, I., Leblanc, B., Wu, X., Johansen, J.V., and Helin, K. (2014). Gene silencing triggers polycomb repressive complex 2 recruitment to CpG islands genome wide. Mol. Cell *55*, 347–360.

Rinn, J.L., and Chang, H.Y. (2012). Genome regulation by long noncoding RNAs. Annu. Rev. Biochem. *81*, 145–166.

Ritchie, M.E., Phipson, B., Wu, D., Hu, Y., Law, C.W., Shi, W., and Smyth, G.K. (2015). limma powers differential expression analyses for RNA-sequencing and microarray studies. Nucleic Acids Res. *43*, e47.

Rivers, C., Idris, J., Scott, H., Rogers, M., Lee, Y.B., Gaunt, J., Phylactou, L., Curk, T., Campbell, C., Ule, J., et al. (2015). iCLIP identifies novel roles for SAFB1 in regulating RNA processing and neuronal function. BMC Biol. *13*, 111.

Robinson, M.D., and Oshlack, A. (2010). A scaling normalization method for differential expression analysis of RNA-seq data. Genome Biol. *11*, R25.

Saldaña-Meyer, R., González-Buendía, E., Guerrero, G., Narendra, V., Bonasio, R., Recillas-Targa, F., and Reinberg, D. (2014). CTCF regulates the human p53 gene through direct interaction with its natural antisense transcript, Wrap53. Genes Dev. *28*, 723–734.

Saldaña-Meyer, R., Rodriguez-Hernaez, J., Escobar, T., Nishana, M., Jácome-López, K., Nora, E.P., Bruneau, B.G., Tsirigos, A., Furlan-Magaril, M., Skok, J., and Reinberg, D. (2019). RNA Interactions Are Essential for CTCF-Mediated Genome Organization. Mol. Cell *76*, 412–422.e5.

Savell, K.E., Gallus, N.V., Simon, R.C., Brown, J.A., Revanna, J.S., Osborn, M.K., Song, E.Y., O'Malley, J.J., Stackhouse, C.T., Norvil, A., et al. (2016). Extra-coding RNAs regulate neuronal DNA methylation dynamics. Nat. Commun. *7*, 12091.

Sedore, S.C., Byers, S.A., Biglione, S., Price, J.P., Maury, W.J., and Price, D.H. (2007). Manipulation of P-TEFb control machinery by HIV: recruitment of P-TEFb from the large form by Tat and binding of HEXIM1 to TAR. Nucleic Acids Res. *35*, 4347–4358.

Shannon, P., Markiel, A., Ozier, O., Baliga, N.S., Wang, J.T., Ramage, D., Amin, N., Schwikowski, B., and Ideker, T. (2003). Cytoscape: a software environment for integrated models of biomolecular interaction networks. Genome Res. *13*, 2498–2504.

Sigova, A.A., Abraham, B.J., Ji, X., Molinie, B., Hannett, N.M., Guo, Y.E., Jangi, M., Giallourakis, C.C., Sharp, P.A., and Young, R.A. (2015). Transcription factor trapping by RNA in gene regulatory elements. Science *350*, 978–981.

Skalska, L., Beltran-Nebot, M., Ule, J., and Jenner, R.G. (2017). Regulatory feedback from nascent RNA to chromatin and transcription. Nat. Rev. Mol. Cell Biol. *18*, 331–337.

Smedley, D., Haider, S., Ballester, B., Holland, R., London, D., Thorisson, G., and Kasprzyk, A. (2009). BioMart–biological queries made easy. BMC Genomics *10*, 22.

St Laurent, G., Shtokalo, D., Tackett, M.R., Yang, Z., Eremina, T., Wahlestedt, C., Urcuqui-Inchima, S., Seilheimer, B., McCaffrey, T.A., and Kapranov, P. (2012). Intronic RNAs constitute the major fraction of the non-coding RNA in mammalian cells. BMC Genomics *13*, 504.

Stock, J.K., Giadrossi, S., Casanova, M., Brookes, E., Vidal, M., Koseki, H., Brockdorff, N., Fisher, A.G., and Pombo, A. (2007). Ring1-mediated ubiquitination of H2A restrains poised RNA polymerase II at bivalent genes in mouse ES cells. Nat. Cell Biol. *9*, 1428–1435.

Studniarek, C., Tellier, M., Martin, P.G.P., Murphy, S., Kiss, T., and Egloff, S. (2021). The 7SK/P-TEFb snRNP controls ultraviolet radiation-induced transcriptional reprogramming. Cell Rep. *35*, 108965.

Szklarczyk, D., Gable, A.L., Lyon, D., Junge, A., Wyder, S., Huerta-Cepas, J., Simonovic, M., Doncheva, N.T., Morris, J.H., Bork, P., et al. (2019). STRING v11: protein-protein association networks with increased coverage, supporting functional discovery in genome-wide experimental datasets. Nucleic Acids Res. *47* (D1), D607–D613.

Tie, C.H., Fernandes, L., Conde, L., Robbez-Masson, L., Sumner, R.P., Peacock, T., Rodriguez-Plata, M.T., Mickute, G., Gifford, R., Towers, G.J., et al. (2018). KAP1 regulates endogenous retroviruses in adult human cells and contributes to innate immune control. EMBO Rep. *19*, e45000.

Trendel, J., Schwarzl, T., Horos, R., Prakash, A., Bateman, A., Hentze, M.W., and Krijgsveld, J. (2019). The Human RNA-Binding Proteome and Its Dynamics during Translational Arrest. Cell *176*, 391–403.e19.

Tsai, P.F., Dell'Orso, S., Rodriguez, J., Vivanco, K.O., Ko, K.D., Jiang, K., Juan, A.H., Sarshad, A.A., Vian, L., Tran, M., et al. (2018). A Muscle-Specific Enhancer RNA Mediates Cohesin Recruitment and Regulates Transcription In trans. Mol. Cell *71*, 129–141.e8.

UniProt Consortium (2019). UniProt: a worldwide hub of protein knowledge. Nucleic Acids Res. *47* (D1), D506–D515.

Wang, K.C., Yang, Y.W., Liu, B., Sanyal, A., Corces-Zimmerman, R., Chen, Y., Lajoie, B.R., Protacio, A., Flynn, R.A., Gupta, R.A., et al. (2011). A long noncoding RNA maintains active chromatin to coordinate homeotic gene expression. Nature *472*, 120–124.

Wang, X., Goodrich, K.J., Gooding, A.R., Naeem, H., Archer, S., Paucek, R.D., Youmans, D.T., Cech, T.R., and Davidovich, C. (2017a). Targeting of Polycomb Repressive Complex 2 to RNA by Short Repeats of Consecutive Guanines. Mol. Cell *65*, 1056–1067.e5.

Wang, X., Paucek, R.D., Gooding, A.R., Brown, Z.Z., Ge, E.J., Muir, T.W., and Cech, T.R. (2017b). Molecular analysis of PRC2 recruitment to DNA in chromatin and its inhibition by RNA. Nat. Struct. Mol. Biol. *24*, 1028–1038.

Wei, P., Garber, M.E., Fang, S.M., Fischer, W.H., and Jones, K.A. (1998). A novel CDK9-associated C-type cyclin interacts directly with HIV-1 Tat and mediates its high-affinity, loop-specific binding to TAR RNA. Cell *92*, 451–462.

Werner, M.S., and Ruthenburg, A.J. (2015). Nuclear Fractionation Reveals Thousands of Chromatin-Tethered Noncoding RNAs Adjacent to Active Genes. Cell Rep. *12*, 1089–1098.

Wickham, H. (2016). ggplot2: Elegant Graphics for Data Analysis (Springer).

Xue, Y., Pradhan, S.K., Sun, F., Chronis, C., Tran, N., Su, T., Van, C., Vashisht, A., Wohlschlegel, J., Peterson, C.L., et al. (2017). Mot1, Ino80C, and NC2 Function Coordinately to Regulate Pervasive Transcription in Yeast and Mammals. Mol. Cell *67*, 594–607.e4.

Yik, J.H., Chen, R., Nishimura, R., Jennings, J.L., Link, A.J., and Zhou, Q. (2003). Inhibition of P-TEFb (CDK9/Cyclin T) kinase and RNA polymerase II transcription by the coordinated actions of HEXIM1 and 7SK snRNA. Mol. Cell *12*, 971–982.

Zhang, Q., McKenzie, N.J., Warneford-Thomson, R., Gail, E.H., Flanigan, S.F., Owen, B.M., Lauman, R., Levina, V., Garcia, B.A., Schittenhelm, R.B., et al. (2019). RNA exploits an exposed regulatory site to inhibit the enzymatic activity of PRC2. Nat. Struct. Mol. Biol. *26*, 237–247.

Zhao, L., Guo, H., Zhou, B., Feng, J., Li, Y., Han, T., Liu, L., Li, L., Zhang, S., Liu, Y., et al. (2016). Long non-coding RNA SNHG5 suppresses gastric cancer progression by trapping MTA2 in the cytosol. Oncogene *35*, 5770–5780.

Zoabi, M., Nadar-Ponniah, P.T., Khoury-Haddad, H., Usaj, M., Budowski-Tal, I., Haran, T., Henn, A., Mandel-Gutfreund, Y., and Ayoub, N. (2014). RNA-dependent chromatin localization of KDM4D lysine demethylase promotes H3K9me3 demethylation. Nucleic Acids Res. *42*, 13026–13038.

STAR★METHODS

KEY RESOURCES TABLE

REAGENT or RESOURCE	SOURCE	IDENTIFIER
Antibodies		
DNMT3A	Abcam	Cat# ab285;, RRID:AB_303355
TRRAP	Abcam	Cat# ab73546; RRID:AB_10672042
LMNA	Abcam	Cat# ab26300; RRID:AB_775965
HMGN1	Bethyl Laboratories	Cat# A302-363A; RRID:AB_1907246
UTF1	Abcam	Cat# ab24273; RRID:AB_778767
CDK9	Abcam	Cat# ab6544; RRID:AB_305557
Beta-Tubulin	Abcam	Cat# ab6046; RRID:AB_2210370
Beta-Actin	Cell Signaling Technology	Cat# 4967; RRID:AB_330288
RUVBL2	Abcam	Cat# ab36569; RRID:AB_2301439
SF3A3	Bethyl Laboratories	Cat# A302-506A; RRID:AB_1966116
ZFP57	Abcam	Cat# ab45341; RRID:AB_946192
FUS	Novus Biologicals	Cat# NB 100-565; RRID:AB_523761
ILF3	Abcam	Cat# ab92355; RRID:AB_2049804
CyclinT1	Abcam	Cat# ab184703; RRID:AB_2814653
UBTF	Santa Cruz	Cat# sc-13125; RRID:AB_671403
KAP1/TRIM28	Abcam	Cat# ab3831; RRID:AB_304099
SUZ12	Santa Cruz	Cat# sc-46264; RRID:AB_2196857
HNRNPU	Abcam	Cat# ab10297; RRID:AB_297037
EHMT1	Abcam	Cat# ab41969; RRID:AB_732115
STAG1	Abcam	Cat# ab4457; RRID:AB_2286589
STAG2	Abcam	Cat# ab4463; RRID:AB_304471
SMARCC1	Abcam	Cat# ab172638
BRD4	Santa Cruz	Cat# sc-48772; RRID:AB_2065729
INO80	ProteinTech	Cat# 18810-1-AP; RRID:AB_10598463
CHD1	Cell Signaling Technology	Cat# 4351; RRID:AB_11179073
CHD4	Abcam	Cat# ab70469; RRID:AB_2229454
CHD8	Bethyl Laboratories	Cat# A301-224A; RRID:AB_890578
P300	Santa Cruz	Cat# SC-585; RRID:AB_2231120
KDM2A	Bethyl Laboratories	Cat# A301-475A; RRID:AB_999558
LEO1	Bethyl Laboratories	Cat# A300-174A; RRID:AB_309451
MPP8	Santa Cruz	Cat# sc-398598
SMARCA5	Abcam	Cat# ab3749; RRID:AB_2191856
INST11	Bethyl Laboratories	Cat# A301-274A; RRID:AB_937779
Pol II S2P	Abcam	Cat# ab5095; RRID:AB_304749
Pol II S5P	Millipore	Cat# 05-623; RRID:AB_309852
Total Pol II	Santa Cruz	Cat# sc-899; RRID:AB_632359
Histone H3	Abcam	Cat# ab1791; RRID:AB_302613
LARP7	Bethyl Laboratories	Cat# A303-723A; RRID:AB_11205813
CDK9 (for CLIP/iCLIP)	Santa Cruz	Cat# sc-484; RRID:AB_2275986
CyclinT1 (for CLIP & coIP)	Abcam	Cat# ab238940
Non-specific IgG	Abcam	Cat# ab46540; RRID:AB_2614925
FLAG antibody	Sigma	Cat# F3165; RRID:AB_259529
γH2A.X (Ser139) (clone JBW301)	Sigma	Cat# 05-636-I; RRID:AB_2755003

Continued

REAGENT or RESOURCE	SOURCE	IDENTIFIER
Bacterial and virus strains		
E. coli BL21	N/A	N/A
Chemicals, peptides, and recombinant proteins		
Triptolide	Sigma	Cat# T3652
Flavopiridol hydrochloride hydrate	Sigma	Cat# F3055
Pladienolide B	Santa Cruz	Cat# sc-391691
SUPERase.In	Invitrogen	Cat# AM2694
RNaseA	Sigma	Cat# R6513
Benzonase	Sigma	Cat# E1014
RNaseOUT	Invitrogen	Cat# 1077019
Yeast tRNA	Invitrogen	Cat# AM7119
Iodoacetamide	Sigma	Cat# I1149
Trypsin	Promega	Cat# V5113
Streptavidin Dynabead T1	Invitrogen	Cat# 65601
DNase Turbo	Ambion	Cat# AM2238
RNase I	Ambion	Cat# AM2294
Dynabeads protein G	Invitrogen	Cat# 10003D
SYBR Green I	Invitrogen	Cat# S7585
TRIsure	Bioline	Cat# BIO-38033
TRI Reagent	Sigma	Cat# T3934
SuperScript III Reverse Transcriptase	Invitrogen	Cat# 18080044
ImProm-II Reverse Transcription System	Promega	Cat# A3800
SN-38	Sigma	Cat# H0165
Viability Dye eF780	Invitrogen	Cat# 65-0865-14
Doxorubicin	Sigma	Cat# D1515
Critical commercial assays		
Pierce BCA	Thermo Scientific	Cat# 23225
KAPA Universal Library Quantification kit	Roche	Cat# KK4824
Amaxa Mouse ES Cell Nucleofector kit	Lonza	Cat# VPH-1001
QuantiTect SYBR Green PCR kit	QIAGEN	Cat# 204143
Vybrant FAM Caspase-3 and −7 assay kit	Invitrogen	Cat# V35118
Deposited data		
SILAC proteomics data	This paper	PRIDE: PXD018706
Label-free proteomics data	This paper	PRIDE: PXD018641
iCLIP data	This paper	GEO: GSE150677
RNA-seq data	This paper	GEO: GSE150677
Raw image files	This paper	Mendeley Data: https://doi.org/10.17632/67dcgtbks5.12
Experimental models: Cell lines		
E14 ESC	Hooper et al., 1987	RRID:CVCL_C320
WT HAP1	Studniarek et al., 2021	RRID:CVCL_Y019
7SK KO HAP1	Studniarek et al., 2021	N/A
WT HEK293T	Tie et al., 2018	RRID:CVCL_0063
KAP1 KO HEK293T	Tie et al., 2018	N/A
Oligonucleotides		
7SK F 5′-AGAACGTAGGGTAGTCAAGC-3′	Kanhere et al., 2010	N/A
7SK R 5′-AGAAAGGCAGACTGCCACAT-3′	Kanhere et al., 2010	N/A
Actb F 5′-TCTTTGCAGCTCCTTCGTTG-3′	Stock et al., 2007	N/A

(Continued on next page)

Continued

REAGENT or RESOURCE	SOURCE	IDENTIFIER
Actb R 5′-ACGATGGAGGGGAATACAGC-3′	Stock et al., 2007	N/A
5S rRNA F 5′-AAGCCTACAGCACCCGGTAT-3′	Kanhere et al., 2010	N/A
5S rRNA R 5′-GATCTCGGAAGCTAAGCAGG-3′	Kanhere et al., 2010	N/A
7SK ASO	Flynn et al., 2016	N/A
Scrambled ASO	Flynn et al., 2016	N/A
Software and algorithms		
MaxQuant v1.6.0.13	Cox and Mann, 2008	RRID:SCR_014485
TMM	Robinson and Oshlack, 2010	N/A
Limma	Kammers et al., 2015; Ritchie et al., 2015	RRID:SCR_010943
g:Profiler2 v1.2	Raudvere et al., 2019	RRID:SCR_018190
Ensembl BioMart	Smedley et al., 2009	RRID:SCR_010714
HGNC multi-symbol checker	https://www.genenames.org/tools/multi-symbol-checker/	RRID:SCR_002827
CORUM v3.0	Giurgiu et al., 2019	RRID:SCR_002254
Cytoscape v3.5	Shannon et al., 2003	RRID:SCR_003032
STRING v11	Szklarczyk et al., 2019	RRID:SCR_005223
iCount	König et al., 2010 https://github.com/tomazc/iCount	RRID:SCR_016712
bowtie2 version 2.1.0	Langmead and Salzberg, 2012	RRID:SCR_016368
MISO	Katz et al., 2010	RRID:SCR_003124
STAR version 2.7.3a	Dobin et al., 2013	RRID:SCR_004463
DeepTools version 3.0.2	Ramírez et al., 2016	RRID:SCR_016366
featureCounts version 5.25	Liao et al., 2014	RRID:SCR_012919
DEseq2	Love et al., 2014	RRID:SCR_015687
ggplot2	Wickham, 2016	RRID:SCR_014601
AmiGO 2	http://amigo.geneontology.org/amigo	RRID:SCR_002143

RESOURCE AVAILABILITY

Lead contact
Further information and requests for resources and reagents should be directed to and will be fulfilled by the lead contact, Richard G. Jenner (r.jenner@ucl.ac.uk).

Materials availability
This study did not generate new unique reagents.

Data and code availability
The SILAC and label-free mass spectrometry proteomics data have been deposited to the ProteomeXchange Consortium via the PRIDE (Perez-Riverol et al., 2019) partner repository with the dataset identifiers PRIDE: PXD018706 and PRIDE: PXD018641, respectively. iCLIP and RNA-seq data have been deposited in the Gene Expression Omnibus (GEO) with accession code GEO: GSE150677. Raw immunoblotting and autoradiogram images have been deposited in Mendeley Data: https://doi.org/10.17632/67dcgtbks5.12.

EXPERIMENTAL MODEL AND SUBJECT DETAILS

All cells were cultured at 37°C in 5% CO_2. Cell lines were not authenticated. Mouse E14 ESC (male) (Hooper et al., 1987) were maintained on 0.1% gelatin in KO-DMEM, 10% FCS, 5% knockout serum replacement, non-essential amino acids, L-glutamine, 2-mercaptoethanol, penicillin-streptomycin and 1000 U/ml leukemia inhibitory factor (Amsbio #AMS-263-100). For Pol II inhibition and

nucleosome IP mass spectrometry studies, media was supplemented with 100 mg/l lysine K8 CNLM-291-H, 100 mg/l arginine R10 CNLM-539-H or 100 mg/l light amino acids (K0 and R0) (ThermoFisher #89989 #89987), and 100 mg/l proline. Cells were maintained for 6 passages (~14 doublings) to ensure full amino acid incorporation and were assayed for alkaline phosphatase activity (ThermoFisher #A14353). WT and 7SK KO HAP1 cells (haploid male) (kind gift from Sylvain Egloff; Studniarek et al., 2021) were maintained in Iscove's Modified Dulbecco's Medium (IMDM) with 10% FCS and penicillin/streptomycin. WT and KAP KO HEK293T cells (female; kind gift from Helen Rowe; Tie et al., 2018) were maintained in DMEM, 10% FCS and penicillin-streptomycin. ESC, HAP1 and HEK293T cells were incubated at 37°C and treated with triptolide (10 μM, Sigma T3652), flavopiridol (10 μM, Sigma F3055), or an equivalent volume of DMSO, for the times indicated. For reversal of transcriptional inhibition induced by flavopiridol, after 3 hr of treatment, ESC were washed twice with warm medium and incubated for a further 3 hr. ESC were treated with 1 μM pladienolide B (Santa Cruz sc-391691) or an equal volume of DMSO for 6 hr.

METHOD DETAILS

Experiments were not performed blinded. Samples were not randomized.

Cell fractionation for proteomics experiments

For the Pol II inhibition experiments, heavy and light labeled ESC were treated with triptolide and flavopiridol as described above. For the RNA degradation experiments, RNaseA treatment was performed as described (Beltran et al., 2016). ESC were trypsinized, washed twice with PBS, permeabilized with 0.05% Tween-20 in PBS for 10 min on ice, washed once, resuspended with PBS and mock-treated with 1 U/μl SUPERase.In (Invitrogen AM2694) or treated with 1 μg/μl RNaseA (Sigma R6513) for 30 min at RT. Chromatin fractions were then purified as described (Monte et al., 2012). Cells were then centrifuged at 1200 rpm, washed twice with PBS, and re-suspended in a hypotonic lysis buffer, (10 mM Tris pH 7.5, 15 mM NaCl, 0.15% v/v NP-40) with protease and phosphatase inhibitors (10 mM sodium butyrate, 0.1 mM PMSF, 0.2 mM Na$_3$VO$_4$, 0.1 mM NaF, Complete protease inhibitor and 1 U/ μl Superase.In) and incubated on ice for 5 min. Cells were then centrifuged at 4,000 rpm for 5 min at 4°C and the cytoplasmic supernatant harvested. The nuclear pellet was re-suspended in hypotonic lysis buffer and layered gently onto a sucrose cushion (24% sucrose (w/v), 10 mM Tris pH 7.5, 15 mM NaCl with protease/phosphatase inhibitors and 1 U/μl Superase.In), centrifuged for 10 min at 5,000 rpm and washed with PBS. Isolated nuclei were then resuspended in 20 mM HEPES (pH 7.6), 7.5 mM MgCl$_2$, 30 mM NaCl, 1 M urea, 1% NP-40 with protease/phosphatase inhibitor and 1 U/μl Superase.In and incubated for 10 min on ice to extract soluble proteins. Samples were then centrifuged at 13,000 rpm for 10 min to pellet the insoluble chromatin and the soluble nucleoplasmic fraction removed. The chromatin pellet was washed with PBS and proteins extracted in 50 mM Tris (pH 8), 1 mM EDTA, 0.05% SDS with protease/phosphatase inhibitors and treated with 250 units of benzonase (Sigma E1014) in the presence of 2 mM MgCl$_2$ for 1 hr. Buffer was then added to give a final concentration of 50 mM Tris (pH 8), 10 mM EDTA, 1% SDS with protease/phosphatase inhibitors and incubated at RT for 10 min. Insoluble material was removed by centrifugation at 13,000 g for 15 mins at 4°C and the supernatant harvested.

Nucleosome affinity purification for proteomics

Heavy and light labeled ESC were trypsinised, collected by centrifugation and washed with PBS. Cell pellets were resuspended in 10 volumes of hypertonic buffer (10 mM HEPES pH 7.9, 1.5 mM MgCl$_2$, 10 mM KCl, 0.5 mM DTT and Complete protease inhibitor) for 10 mins on ice. Cells were recovered by centrifugation at 1500 g for 5 mins and the pellet resuspended in 3 volumes of hypertonic buffer supplemented with 0.1% IGEPAL CA-360 and incubated for 10 mins at 4°C. Nuclei were pelleted by centrifugation at 1500 g for 5 mins and resuspended in 5 mM HEPES pH 7.9, 26% glycerol, 250 mM NaCl, 1.5 mM MgCl$_2$, 0.2 mM EDTA, 0.5 mM DTT and Complete protease inhibitor. The NaCl concentration was then slowly increased to 400 mM and nuclear extraction carried out for 1 hr at 4°C with occasional agitation. Insoluble material was removed by centrifugation (13.000rpm, 20 min at 4°C) and soluble nuclear extracts cleared using a Proteus clarification column (Generon #MSF500). Protein concentration was measured using Pierce BCA (ThermoFisher Scientific 23225). Nuclear extracts were then treated with 1 μg/μl RNaseA (Sigma R6513) or mock treated with PBS with 1 U/μl RNaseOUT (Invitrogen 1077019) for 30 mins at 1100 rpm at 37°C. The RNaseA treated sample was then split and half treated with 1 U/μl RNaseOUT and half with 1 U/μl RNaseOUT and 2 μg/μl tRNA (Invitrogen AM7119). Histone octamers were assembled into dinucleosomes by salt deposition dialysis using a biotinylated 382 bp DNA fragment containing the 601 nucleosome-positioning sequence, as described (Makowski et al., 2018). 2.5 μg of dinucleosomes were incubated with 12.5 μL of previously washed Streptavidin Dynabead T1 (Invitrogen 65601) in SNAP Buffer (20 mM HEPES pH 7.9, 150 mM NaCl, 0.2 mM EDTA (pH 8.0), 1 mM DTT, 20% Glycerol, 0.1%, IGEPAL CA-630, plus Complete protease inhibitor) for 1 hr at 4°C. Complexes were washed twice in SNAP buffer and then incubated with 1.2 mg of mock-treated or RNaseA-treated nuclear extract in SNAP buffer with a final volume of 1 ml. The binding reaction was allowed to proceed for 3 hr at 4°C, beads were then washed twice in SNAP buffer and twice in SNAP buffer without IGEPAL CA-630. Nucleosomes were resuspended in 50 μl elution buffer (100 mM Tris pH 7.5, 2 M Urea, 10 mM DTT) and incubated for 20 mins at 25°C at 1100 rpm.

SILAC

For the Pol II inhibition experiments, protein extracts were quantified by BCA. 25 μg of heavy and light labeled samples were mixed to give a total of 50 μg protein. 25 μg of heavy or light-labeled flavopiridol or triptolide-treated samples were mixed with DMSO-treated

samples from the same time point labeled with the alternative amino acids. Heavy labeled samples were also mixed with the equivalent light labeled samples as controls. Heavy or light-labeled flavopiridol washout samples were mixed with alternatively-labeled 3 hr flavopiridol, 3 hr DMSO or washout samples. Mixes were loaded onto separate lanes of a 10% NuPAGE gel (Invitrogen) and run approx. 10 mm. Each lane was manually excised, diced into $\sim$1 mm^3 pieces and transferred to a single well of a flat-bottomed 96-well plate. A Janus liquid handling robot (Perkin Elmer) was used to de-stain, reduce (10 mM dithiothreitol) and alkylate (55 mM iodoacetamide) proteins prior to overnight trypsin digest (100 ng, Pierce Trypsin Protease, MS Grade) at 37°C. The following day, peptides were extracted using 50% acetonitrile, 1% formic acid. Peptide samples were dried by vacuum centrifugation then re-solubilised in 0.1% trifluoroacetic acid prior to mass spectrometry analysis.

For the nucleosome affinity purification experiments, equal volumes of affinity-purified proteins from the heavy or light-labeled RNaseA-treated samples were mixed with the proteins purified from the alternatively-labeled mock-treated samples or with alternatively-labeled RNaseA treated samples as controls. Iodoacetamide (Sigma I1149) was added to a final concentration of 50 mM and samples incubated for a further 10 mins at 25°C at 1100 rpm in the dark. Proteins were digested by addition of 0.3 μg trypsin (Promega V5113) at 25°C for 2 hr at 1100 rpm. Samples were pelleted, the supernatant collected and a second trypsinization performed using 50 μl of elution buffer for 5 mins at 25°C. The supernatant was again collected, combined with the previous sample, and digested by incubation with 0.3 μg of trypsin overnight at 25°C and 1100 rpm. The reaction was then stopped with 0.5% TFA (Sigma), samples desalted using C18 Stage tips and eluted in 60% acetonitrile.

A Thermo Fisher Scientific UltiMate 3000 UHPLC instrument loaded peptide samples onto a trap cartridge (Acclaim PepMap 100 C18, 300 μm inner diameter, 5 mm length, 5 μm particle size) for desalting. Peptides were transferred to an EASY-Spray analytical column (PepMap C18, 50 μm inner diameter, 15 cm length, 2 μm particle size, 100 Å pore size) and separated using a 120-minute gradient of increasing organic solvent (80% acetonitrile, 5% dimethyl sulfoxide) from 8 to 40%. An orbitrap Fusion Lumos Tribrid (Thermo Fisher Scientific) mass spectrometer was operated in positive ionisation mode to acquire data. Instrument settings were: MS1 data were acquired in the orbitrap at a resolution of 120k, 4E6 AGC target, 50 ms maximum injection time, dynamic exclusion of 60 s, a mass range of 300-1500 m/z and profile mode data capture. MS2 data were acquired in the ion trap using a 2 m/z isolation window, 2E4 AGC target, 300 ms maximum injection time (inject ions for all available parallelisable time "Universal Method"), 35% collision-induced dissociation (CID) energy, 10 ms activation time and centroid mode data capture.

Label-free quantification (LFQ)

Chromatin fractions from RNaseA-treated and mock-treated cells were collected from 4 independent experiments, loaded onto separate wells of a NuPAGE gel (Invitrogen) and run until fully resolved. The gel was cut horizontally into five sections to facilitate quantification by molecular weight across lanes. Bands from each lane were excised and diced into 1 mm^3 pieces. Gel pieces were washed with 50% acetonitrile and water. Proteins were reduced with 10 mM dithiothreitol in 100 mM ammonium bicarbonate at 56°C for 45 min and alkylated with 55 mM iodoacetamide in 100 mM ammonium bicarbonate at ambient temperature for 30 mins in the dark. Gel pieces were washed again as before. Proteins were digested with 300 ng trypsin at 37°C overnight. Peptides were extracted with 50% and 100% acetonitrile washes. Samples were evaporated to dryness at 30°C and resolubilised in 0.1% formic acid. LC-MS/MS was performed on a Q Exactive Orbitrap Plus interfaced to a NANOSPRAY FLEX ion source and coupled to an Easy-nLC 1200 (Thermo Scientific). Thirty five percent of each sample was analyzed as 7 μl injections. Peptides were separated on a 24 cm fused silica emitter, 75 μm diameter, packed in-house with Reprosil-Pur 200 C18-AQ, 2.4 μm resin (Dr. Maisch) using a linear gradient from 5% to 30% acetonitrile/0.1% formic acid over 120 min at a flow rate of 250 nl/min. Peptides were ionised by electrospray ionisation using 1.8 kV applied immediately prior to the analytical column via a microtee built into the nanospray source with the ion transfer tube heated to 320°C and the S-lens set to 60%. Precursor ions were measured in a data-dependent mode in the orbitrap analyzer at a resolution of 70,000 and a target value of 3e6 ions. The ten most intense ions from each MS1 scan were isolated, fragmented in the HCD cell, and measured in the orbitrap at a resolution of 17,500.

Cell fractionation for validation experiments

To validate changes in chromatin association upon Pol II inhibition and RNA degradation detected by LC-MS/MS, ESC were treated with triptolide, flavopiridol or RNaseA as described above. Cell fractionation was performed as described previously (Beltran et al., 2016; Zoabi et al., 2014). Cells were centrifuged at 1200 rpm, washed twice with PBS and 20% of the cells separated for use as WCE. The remaining cells were re-suspended in 1 mL of buffer A (10 mM HEPES (pH 7.9), 10 mM KCl, 1.5 mM MgCl2, 0.34 M sucrose, 10% glycerol, 1 mM DTT with Complete protease inhibitor). Triton X-100 (0.1%) was added, and the cells were incubated for 5 min on ice. Nuclei were collected by low-speed centrifugation (4 min, 1,300 g, 4°C). The supernatant (cytoplasmic fraction) was further clarified by high-speed centrifugation (15 min, 20,000 g, 4°C). Nuclei were washed twice in buffer A, and then lysed in buffer B (3 mM EDTA, 0.2 mM EGTA, 1 mM DTT, Complete protease inhibitor). Insoluble chromatin was collected by centrifugation (4 min, 1,700 g, 4°C), and the supernatant (nucleoplasm) harvested. The final chromatin pellet (insoluble chromatin fraction) was washed twice with buffer B and proteins extracted in 50 mM Tris (pH 8), 1 mM EDTA, 0.05% SDS with Complete protease inhibitor and 250 units of benzonase in the presence of 2 mM MgCl$_2$ for 1 hr. Buffer was then added to give a final concentration of 50 mM Tris (pH 8), 10 mM EDTA, 1% SDS with Complete protease inhibitor and incubated at RT for 10 min. Insoluble material was removed by centrifugation at 13,000 g for 15 mins at 4°C and the supernatant harvested. The experiments were performed in duplicate.

Nucleosome affinity purification validation

Recombinant human histones were expressed in *E. coli* and purified as described (Makowski et al., 2018). Histone octamers were assembled into mononucleosomes and dinucleosomes by salt deposition dialysis using biotinylated 147, 185 and 382 bp DNA fragments containing the 601 nucleosome-positioning sequence. 1.25 μg dinucleosomes pre-bound to Streptavidin Dynabead T1 or equimolar amount of mononucleosomes were incubated with 50 μg of mock or RNaseA-treated nuclear extract in SNAP buffer with a final volume of 250 μl. The binding reaction was allowed to proceed for 3 hr at 4°C, beads were then washed 3 times in SNAP buffer and nucleosomes resuspended in NuPAGE protein loading buffer. The experiment was performed in duplicate.

Immunoblotting

Cell fractions and extracts were quantified by BCA (Pierce). Samples were boiled in Laemmli buffer or NuPAGE buffer and equal amounts (10 μg) of cell fractions (equal volumes for immunoprecipitates) were loaded for each treatment. When blotting for Pol II phospho-forms, cells were lysed in TOPEX+ buffer (50 mM Tris-HCl pH7.5. 300 mM NaCl, 0.5% Triton X-100, 1% SDS, 1 mM DTT, 1x Complete protease inhibitor (Roche), 5 mM NaF, 0.2 mM Na_3VO_4, 10 mM β-glycerophosphate, and 33 U/ml benzonase (EMD-Novagen). Proteins were resolved by SDS-PAGE with size markers (ThermoFisher) and transferred to nitrocellulose membranes (GE Healthcare). Proteins were detected with primary antibodies to DNMT3A (Abcam ab2850), TRRAP (Abcam ab73546), SET (Abcam ab181990), LMNA (Abcam ab26300), HMGN1 (Bethyl Laboratories A302-263), UTF1 (Abcam ab24273), CDK9 (Abcam ab6544), beta-Tubulin (Abcam ab6064), RUVBL2 (Abcam ab36569), SF3A3 (Bethyl Laboratories A302-506A), ZFP57 (Abcam ab45341), FUS (Novus Biologicals 100-565), LARP7 (Novus biologicals A303-723A), ILF3 (Abcam ab92355), CyclinT1 (Abcam ab184703), UBTF (Santa Cruz sc-13125), KAP1/TRIM28 (Abcam ab3831), SUZ12 (Santa Cruz sc-46264), LEO1 (Bethyl Laboratories A300-174A), HNRNPU (Abcam ab10297), EHMT1 (Abcam ab41969), STAG1 (Abcam ab4457), STAG2 (Abcam 4463), SMARCC1 (Abcam ab172638), BRD4 (Santa Cruz sc-48772), INO80 (ProteinTech 18810-1-AP), CHD1 (Cell Signaling D8C2), CHD4 (Abcam ab70369), CHD8 (Bethyl A301-224A), P300 (Santa Cruz sc-585), KDM2A/JHDM1A (Bethyl A301-475A), MPP8 (Santa Cruz sc-398598), Pol II S2P (Abcam ab5095), Pol II S5P (Millipore 05-623), total Pol II (Santa Cruz sc-899), Beta-actin (Cell Signaling 4967S), histone H3 (Abcam ab1791) and γH2A.X (Ser139) (clone JBW301) (Sigma 05-636-I). Proteins were visualized using Amersham ECL western blotting detection reagent (GE) and detected using an ImageQuantLAS 4000 imager and ImageQuantTL (GE). Contrast and brightness were altered in a linear fashion equally across the whole image. Proteins exhibit changes in chromatin association or nucleosome binding that were not validated by immunoblotting are indicated in Tables S1, S3, and S5.

7SK knockdown

ESC were trypsinized and nucleofected with 1 nmole of scrambled or 7SK ASO (Flynn et al., 2016) per 2x10^6 ESC using the Amaxa 4D-Nucleofector X Unit (Lonza VPH-1001) with the Amaxa 4D-Nucleofector Protocol for Mouse ESC. After nucleofection, cells were re-plated and cultured for 8 hr. RNA was purified using TRIsure (Bioline BIO-38033) according to the manufacturer's instructions and reverse transcribed with SuperScript III (ThermoFisher) using random hexamer primers. Enrichment of cDNAs compared to input control was measured by qPCR (Applied Biosystems) using QuantiTect SYBR Green PCR kit (QIAGEN 204143) with primers for 7SK 5′-AGAACGTAGGGTAGTCAAGC −3′ and 5′- AGAAAGGCAGACTGCCACAT −3′ and Actb 5′-TCTTTGCAGCTCCTTCGTTG-3′ and 5′-ACGATGGAGGGGAATACAGC-3′. The experiment was repeated 7 times.

CLIP

CLIP was performed as described (Huppertz et al., 2014) with the following differences: cells were irradiated with 0.2 J/cm² of 254 nm UV light in a Stratalinker 2400 (Stratagene). 5x10^6 cells were used per IP and were lysed in 1 mL of lysis buffer with Complete protease inhibitor (Roche). Lysates were passed through a 27 G needle, 4 U/ml of DNase Turbo (Ambion AM2238) and RNase I (Ambion AM2294, range between 1-20 U/ml) added, and incubated in a thermomixer at 37°C and 1100 rpm for 3 minutes. 5 μL of α-RUVBlI2 (Abcam ab36569), 5 μg α-UBTF (Santa Cruz sc-13125), 5 μg α-INO80 (ProteinTech 18810-1-AP), α-CHD4 (Abcam ab70369), α-SMARCC1 (Abcam ab172638), α-EHMT1 (Abcam ab41969), α-CDK9 (Santa Cruz sc-484), α-LARP7 (Bethyl A303-723A), α-SMARCA5/SNF2H (Abcam ab3749), α-INTS11 (Bethyl A301-274A), α-CCNT1 (Abcam ab238940), α-CDK9 (Santa Cruz sc-484), α-LARP7 Bethyl A303-723A) or non-specific IgG (Abcam ab46540) antibody was used per experiment and bound to 50 μl of pre-washed Dynabeads protein G beads (Invitrogen 10003D) for 1 hr at RT. Antibody-bound beads were then incubated with lysate for 5 hr at 4°C. Beads were washed 3 times with 900 μl of high-salt buffer (supplemented with 1 M urea) and twice with 900 μl of wash buffer. After transfer, the membrane was washed twice with 1x PBS, exposed overnight to a phosphoimager screen (Fuji), and visualized with an Amersham Typhoon Trio image scanner. Protein and RNA bands were quantified with ImageJ. CLIP experiments were performed in duplicate.

iCLIP

iCLIP was performed as described (Huppertz et al., 2014) with variations from Beltran et al. (2016). Cells were irradiated with 0.2 J/cm² of 254 nm UV light in a Stratalinker 2400 (Stratagene), 6-10x10^7 cells were used per IP. Cells were lysed in 1 mL of lysis buffer, lysates passed through a 27 G needle and sonicated for 3x 10 s pulses with a Diagenode Picoruptor. 200 U/ml of DNase Turbo (Ambion), and 4 U/ml of RNase I (Ambion) were added and lysates incubated in a thermomixer at 37°C and 1100 rpm for 3 mins. Lysates were cleared by centrifugation and Proteus clarification spin columns, according to the manufacturer's instructions. 5 μg of antibody

was used for each CLIP (CDK9 Santa Cruz sc-484; LARP7 Bethyl A303-723A). After SDS-PAGE and transfer to membrane, crosslinked RNPs between 80 and 110 kDa (CyclinT1) or 70 to 100 kDa (LARP7) were isolated. iCLIP for the CyclinT1 input sample was performed as described (Beltran et al., 2016), extracting RNPs between 80-110 kDa. RNA was purified and after reverse transcription, cDNA was fractionated by running samples on a precast 6% TBE-urea gel at 180 V for 40 mins and cDNA bands running between 120-180 nt (high), 85-120 nt (medium) and 70-85 nt (low) isolated. One μl of each fraction was pooled to optimize the number of cycles in the PCR, determined by the minimum number of cycles that produced detectable amplicon in gels stained with SYBR Green I (Invitrogen S7585). Once the optimal number of optimal cycles was established, the library PCR was performed separately for each fraction, checked by gel electrophoresis and pooled in equal proportions. Library concentration was determined using the KAPA Universal Library Quantification kit (Roche KK4824), according to the manufacturer's instructions and library concentration was corrected by multiplication by 0.38 to account for insert size. Single-end 50-bp reads were generated on a HiSeq 2500.

Co-immunoprecipitation from chromatin

ESC were treated with 10 μM triptolide or an equivalent volume of DMSO for 6 hours, trypsinized and the chromatin fraction purified as described (Beltran et al., 2016; Zoabi et al., 2014). Chromatin was resuspended in 50 mM Tris (pH 8), 1 mM EDTA and 20 U/ml of DNase Turbo (Ambion AM2238) for 30 min at RT, followed by the addition of 0.5% sodium deoxycholate and sonication for 10 × 30 s pulses with a Diagenode Picoruptor. Once the chromatin fraction was completely dissolved, IP buffer (20 mM Tris-HCl, 0.5% NP-40, 150 mM NaCl, 1.5 mM MgCl2, 10 mM KCl, 10% Glycerol, 0.5 mM EDTA, pH 7.9, 1 mM DTT, Complete protease inhibitor and 1 U/μl RNaseOUT (Invitrogen 1077019)) was added up to 1 mL and centrifuged for 5 min at 13,000 rpm to pellet any insoluble material. 50 μl of the sample was saved as input and the remaining sample pre-cleared with Protein G Dynabeads at 4°C for 1 hr. The beads were removed, each sample divided into two, and incubated with 2.5 μg of anti-CCNT1 (Abcam ab238940) or non-specific IgG for 16 hours. Samples were then incubated with Protein G Dynabeads at 4°C for 2 hours. Beads were washed 5 times with IP buffer and centrifuged for 5 min at 1,000 rpm at 4°C to remove any remaining supernatant. Laemmli buffer was added to half the beads and inputs and processed for immunoblotting and the other halves were resuspended in TRIsure for RNA purification. RNA was treated with DNase Turbo and reverse-transcribed with the ImProm-II Reverse Transcription System (Promega A3800) using random hexamer primers. Enrichment of 7SK versus 5S rRNA was measured by qPCR (Applied Biosystems) using QuantiTect SYBR Green PCR kit (QIAGEN) with primers for 7SK 5′-AGAACGTAGGGGTAGTCAAGC-3′ and 5′-AGAAAGGCAGACTGCCACAT-3′ and 5S rRNA 5′-AAGCCTACAGCACCCGGTAT-3′ and 5′-GATCTCGGAAGCTAAGCAGG-3′. The experiment was repeated 3 times.

RNA-seq

ESC were mock or RNaseA treated or treated with 10 μM triptolide or flavopiridol for 0, 1, 3 or 9 hours. For whole cell extract RNA, cells were resuspended in TRIsure. For chromatin-associated RNA, cells were fractionated as described (Werner and Ruthenburg, 2015) with minor modifications. Cells were re-suspended in 1 mL of buffer A (10 mM HEPES (pH 7.9), 10 mM KCl, 1.5 mM MgCl2, 0.34 M sucrose, 10% glycerol, 1 mM DTT with Complete protease inhibitor), Triton X-100 (0.1%) added, and the cells were incubated for 5 mins on ice. Nuclei were collected by low-speed centrifugation (4 min, 1,300 g, 4°C) and washed twice in buffer A. The pellet was resuspended in 250 μl NUN buffer (20 mM HEPES pH 7.6, 300 mM NaCl, 1M Urea, 1% NP-40, 7.5 mM MgCl2, 1 mM DTT, with protease inhibitor) and incubated for 10 mins on ice, then centrifuged (1,400 g, 4 min, 4°C). The resulting pellet was washed twice with buffer A and an equal volume of TRI Reagent (Sigma T3934) was added to the chromatin pellet. Before RNA extraction, we spiked-in 5% of *Drosophila* cells resuspended in TRIsure into the whole cell extract RNA samples and 1% into the chromatin-associated RNA samples. RNA was purified following the manufacturer's protocol and treated with DNase Turbo. Libraries were generated from WCE RNA by polyA selection and from chromatin-associated RNA library by rRNA depletion and sequenced by GENEWIZ.

Cell cycle, caspase activation, cell death, γH2A.X

ESC were treated with triptolide or flavopiridol as above, or with 10 nM SN-38 (Sigma H0165) for 24 hr. Cells were then trypsinized and resuspended in media. Cell viability was measured using eF780 (Invitrogen 65-0865-14) in triplicate. Caspase-3 and −7 activation was measured in duplicate using the Vybrant FAM Caspase-3 and −7 assay kit (Invitrogen V35118) following the manufacturer's instructions with a BD LSR Fortessa X-20. For cell cycle analysis, cells were fixed with 70% ethanol, washed with PBS and incubated with 100 μg/ml RNaseA (Sigma) and 25 μg/ml propidium iodide from the sVybrant FAM Caspase kit for 10 mins at RT. Cells were then analyzed by flow cytometry in triplicate and the data averaged. For γH2A.X analysis, cells were treated with triptolide or flavopiridol as above, or with 10 μM doxorubicin (Sigma D1515), and whole cell extract purified. The experiment was performed 3 times.

QUANTIFICATION AND STATISTICAL ANALYSIS

Statistical tests used and n are stated upon first use in the Results text and in the figure legends.

Mass-spectrometry data analysis
SILAC

Raw data were analyzed in MaxQuant v1.6.0.13 (Cox and Mann, 2008) and searched against a UniProt *Mus musculus* protein database downloaded 14/06/2012 using default settings. A SILAC quantification method (multiplicity 2) using light amino acid labels (K0

and R0) and heavy labels (K8 and R10) was selected. Carbamidomethylation of cysteines was set as fixed modification, and oxidation of methionines and acetylation at protein N-termini were set as variable modifications. Enzyme specificity was set to trypsin with maximally 2 missed cleavages allowed. MaxQuant generated a reverse database for decoy searching and an internal protein contaminant database was also searched containing sequences including trypsin and keratins. A 1% FDR at the protein and peptide level was selected.

LFQ

Raw data were analyzed in MaxQuant v1.5.2.8 and searched against the same UniProt database. Label-free quantification was selected with a match time window of 0.7 min, an alignment time window of 20 min to quantify the proteins with the 'match between runs' feature selected. Other settings were the same as for SILAC.

LC-MS/MS data post-processing and analysis

The 'proteinGroups.txt' quantification files were used for statistical data analysis and the Pol II inhibition, RNase-treated chromatin and RNase-treated nucleosome affinity purification experiments processed separately. Proteins marked as *Potential contaminant*, *Only identified by site*, *Reverse* by MaxQuant and proteins with less than two peptides identified were excluded. The remaining proteins were classified into nuclear and non-nuclear proteins based on subcellular location information in UniProt (UniProt Consortium, 2019) as of 2018-12-18. Subcellular locations *Nucleus*, *Nucleus speckle*, *Chromosome*, *Nucleus matrix*, *Nucleus envelope*, *Nucleus inner membrane*, *Nucleus membrane*, *Nucleus outer membrane* were treated as nuclear. Proteins with no localization information were assumed to be nuclear. Non-nuclear proteins were discarded. Intensities (either SILAC-labeled or LFQ) of the remaining proteins were normalized using TMM (Robinson and Oshlack, 2010). For SILAC experiments, log2 protein intensities were converted into log2(H/L) ratios which were compared between forward and reverse experiments. Outlier proteins that did not show typical anticorrelation between forward and reverse H/L ratio in SILAC experiments were detected and removed by estimating the direction of first and second principal components of pooled ratios of significantly enriched proteins in all experiments (forward log2 ratio > 1.25, reverse < −1.25 or vice-versa) and discarding all proteins 2.5-standard deviations away from the median in the second principal direction. This procedure was been performed twice, adjusting the PCA estimates once more after removing outlier proteins. Intensities of remaining proteins were re-normalized again using TMM. The ratio outlier filtering step was skipped in LFQ dataset.

Normalized intensities of remaining proteins were analyzed using Limma (Kammers et al., 2015; Ritchie et al., 2015). Three and nine-hour Pol II inhibition datasets were analyzed separately, as were RNase-treated chromatin and nucleosome affinity purification experiments. SILAC experiments were modeled based on the log2 intensities of proteins, assuming additive treatment (inhibitor versus DMSO or RNase versus Mock) effect, additive mix (SILAC experiment batch) bias, and additive isotope (H/L labeling) bias. The change of intensity after washout of flavopiridol (relative to intensity after 3 hr flavopiridol treatment) was modeled as an additional parameter in three-hour inhibition model. The change of intensity after addition of tRNA (as compared to RNase treatment without tRNA) was modeled similarly in SILAC nucleosome purification experiments. The label-free chromatin RNase treatment dataset was modeled assuming additive treatment effect (RNase versus Mock) and paired experiment batch effects. Limma models were fitted with trend parameter set. Statistical testing was performed on treatment and washout/tRNA terms. P values were adjusted by Benjamini/Hochberg method, significance was assumed at FDR of 0.05. Comparisons between the different experiments were performed by matching the outputs by UniProt protein IDs, discarding rows that map ambiguously. To allow direct comparison to the Pol II inhibition data, only proteins with UniProt protein IDs that were also present in the RNA pol II inhibition dataset were visualized in the RNaseA treatment volcano plots and FDR values were calculated based on the population of proteins that were also detected in the RNA Pol II inhibition experiment.

We identified proteins that were significantly enriched or depleted in the chromatin fraction upon treatment with both flavopiridol and triptolide at 9 hr (FDR < 0.05). To measure the effect of flavopiridol washout, we identified all proteins significantly enriched or depleted on chromatin after 3 hours incubation (FDR < 0.05) that were also detected in the washout experiment (n = 523). We then calculated the Pearson correlation between log2(FP 3hr/DMSO 3hr and log2(washout/FP3hr) and its significance (corr.test in R, which applies a t test). We also identified proteins significantly enriched or depleted in the chromatin fraction after RNaseA treatment (FDR < 0.05) and proteins with significantly increased or decreased binding to nucleosomes after RNA degradation (FDR < 0.05). We took the set of proteins significantly enriched or depleted in the chromatin fraction upon treatment with both flavopiridol and triptolide at 9 hr and calculated the average change in chromatin binding between the two treatments. We then calculated the correlation between these values and the change in chromatin binding caused by RNaseA treatment. The significance of correlations between datasets was estimated using corr.test in R. The significance of overlaps between sets of proteins depleted or enriched on chromatin after Pol II inhibition and RNaseA treatment were compared using the hypergeometric test in R using the set of proteins detected in both treatments as the population.

Gene names were reannotated using the Mouse Genome Informatics (MGI) database and used to perform enrichment analysis against the GO (release 2020-01-01), Reactome (2020-2-7), KEGG (2020-02-03) and WP (20200110) databases using the hypergeometric test in g:Profiler2 v1.2 (Raudvere et al., 2019). Mouse proteins annotated with the terms RNA processing (GO:0006396) or Chromatin organization (GO:0006325) were downloaded from AmiGO 2 (http://amigo.geneontology.org/amigo) and used to identify proteins with these functions in the volcano plots. Mouse gene names were also mapped to human gene names using Ensembl BioMart (http://useast.ensembl.org/biomart/martview/0e2a64a75123489044c7f7866711cb8d). Mouse gene names that did not match

any human gene names using BioMart were checked using HGNC multi-symbol checker (https://www.genenames.org/tools/multi-symbol-checker/) and then mapped to their human gene names. Protein complexes with significant enrichment of subunits in the set of recruited or depleted proteins were identified from CORUM 3.0 (03.09.2018) (Giurgiu et al., 2019) using the hypergeometric test in g:profiler2 v1.2. Subunits missing from CORUM were manually added to the cytoscape figures and a hypergeometric test repeated to ensure the complexes remained significant. Additional complexes or functionally related groups not annotated in CORUM were also added if significant (these were DNMTs, EHMTs, HUSH, NoRC, P-TEFb, SEC and SAFB factors in Figure 1C and PRC1.6 and NSL in Figure 3C). Complexes were depicted using Cytoscape v3.5 (Shannon et al., 2003). Interactions between proteins in these complexes was taken from STRING v11 (Szklarczyk et al., 2019) using experiments as the active interaction source.

iCLIP data analysis

iCLIP data were processed using iCount (https://github.com/tomazc/iCount) as described (Beltran et al., 2019). The unique molecular identifiers (UMIs) were registered and experimental barcodes removed before mapping the sequences to mm9 using Bowtie version 0.12.7 (command line: -v 2 -m 1 -a–best–strata) in iCount. Reads indicative of PCR duplicates (reads mapping to the same position with the same UMI) and reads aligning to multiple positions in the genome were removed. Data from independent replicate samples were then added together (P-TEFb n = 3; LARP7 n = 2, Input n = 1, P-TEFb in pla-B-treated cells n = 1, P-TEFb in DMSO-treated cells n = 1). When mapping crosslinks to genes, crosslinks overlapping a RepeatMasker feature or ncRNAs under 200 nt in length or annotated as a snoRNA were removed. Crosslink sites were assigned to the nearest splice site junction by iCount (Ensembl59 annotation). First exon-intron, mid exon-intron, intron- mid exon and last intron-exon junctions were defined as those uniquely annotated with these designations by Ensembl59. The number of crosslink sites at each position were normalized by the total number of exons or introns at that position and by the total number of crosslink sites in the dataset multiplied by 10^9. The data points were smoothened over a 12-nt sliding window using the smth.Gaussian function from the smoother package in R with smoother.gaussianwindow.alpha = 2.3 and plotted with the ggplot2 package in R. We used MISO (Katz et al., 2010) to identify included exons (posterior mean value > 0.90) and excluded exons (posterior mean value < 0.10) from previously published mESC mRNA-seq data (Beltran et al., 2016). Exon-intron junctions that were also annotated in Ensembl 59 were retained and P-TEFb and input crosslinks over the exon-intron boundaries were normalized, smoothened and plotted as above. When plotting RNA crosslinking at individual genes, high-confidence clusters of crosslink sites were identified using the low FDR function in iCount (FDR < 0.05), with a 50 nt flank (König et al., 2010).

For comparison of P-TEFb RNA crosslinking at single-exon versus multi-exon genes, exon number was identified from the Ensembl 59 annotation. The number of P-TEFb and input RNA crosslinks per gene were normalized by the total number of reads mapping to all the genes and multiplied by a factor of 1 million. For genes with crosslinks in both samples, the log2 ratios (P-TEFb/input) were plotted and a t test performed.

For mapping crosslinks to 7SK and snRNAs, non-transcribed 7SK pseudogenes were masked in the mm9 genome sequence and reads aligned using bowtie2 version 2.1.0 (command line parameters:–very-sensitive–no-unal) (Langmead and Salzberg, 2012). Reads aligning to multiple positions in the genome were removed, but for this analysis, reads mapping to the same position with the same UMI were retained due to the risk of high abundance target RNAs saturating the number of possible UMIs (4^5).

RNA-seq analysis

RNA-Seq data were aligned to concatenated mouse-*Drosophila* genome (mm9 and BDGP5.25 assembly) using STAR (version 2.7.3a) (Dobin et al., 2013). Uniquely mapped reads were extracted from the aligned bam files, which were then split into Mouse and *Drosophila*. The number of reads mapping to the *Drosophila* genome were used to calculate a scaling factor that was then used to scale the Mouse bigwig files generated using deepTools (version 3.0.2) (Ramírez et al., 2016). Exonic and intronic coordinates were extracted from Ensembl 67 annotation and featureCounts (Liao et al., 2014) in R used to count the number of reads in exons or introns for each Mouse gene. The number of reads mapping to a gene in *Drosophila* was counted by featureCounts using a gtf file (version 5.25). DESeq2 (Love et al., 2014) was used to calculate the size-factors for the *Drosophila* reads and these were then used to normalize the read counts mapping to the Mouse genome. A pseudo-count of 1 was added to the data and log2 ratios calculated relative to t = 0 (for Pol II inhibition) or mock (for RNaseA). Gene biotype information was downloaded for Ensembl 67 using BioMart (Smedley et al., 2009). Genes with a non-coding biotype were assigned to lincRNA biotype after manual curation. Cumulative frequency distribution plots were generated from log2 ratios using ggplot2 (Wickham, 2016). Metagene plots were generated using the computeMatrix and plotProfile functions in deepTools.

Comparison to RNA binding studies

Proteins detected to bind RNA in previously published studies were downloaded from (Caudron-Herger et al., 2019) and the data compared to our data using human protein names. Proteins that increase on chromatin upon both 9hrs TRP and FP treatment (FDR < 0.05), proteins that decrease on chromatin upon both 9hrs TRP and FP treatment (FDR < 0.05) and proteins remaining constant on chromatin upon both 9hrs TRP and FP treatment (FDR > 0.05) were identified and the proportion of proteins in each of these sets identified to bind RNA in each study was quantified. The significance of the proportion of proteins that increase and decrease on chromatin identified as RNA binding proteins was estimated relative the proportion of non-changing proteins identified as RNA binding proteins using the Binomial test and the p values adjusted for multiple hypothesis testing to reflect the 12 studies assessed.

CLIP and immunoblotting

P-TEFb (n = 7) and LARP7 (n = 2) RNA crosslinking was quantified in cells treated with 7SK ASO relative to RNA crosslinking in cells treated with scrambled ASO and normalized to change in CyclinT1 or LARP7 protein amount. The mean and SD of these values were then plotted and the significance of the change in RNA crosslinking (7SK/scrambled) estimated using a 1-sided Welch's unequal variance t test.

CyclinT1, CDK9, LARP7 and SMARCC1 chromatin binding was quantified 3 or 6 hr after treatment with triptolide relative to before treatment in the same cell line in triplicate and the mean and SD plotted. The significance of the difference between WT and KO cells at the same time point was estimated using a 1-sided Student's t test.